9. New Developments in Laser Spectroscopy

During the last few years several new ideas have been born and new spectroscopic techniques have been developed that not only improve the spectral resolution and increase the sensitivity for investigating single atoms but that also allow several interesting experiments for testing fundamental concepts of physics. In the historical development of science, experimental progress in the accuracy of measurements has often brought about a refinement of theoretical models or even the introduction of new concepts [9.1]. Examples include A. Einstein's theory of special relativity based on the interferometric experiments of Michelson and Morley [9.2], M. Planck's introduction of quantum physics for the correct explanation of the measured spectral distribution of blackbody radiation, the introduction of the concept of electron spin after the spectroscopic discovery of the fine structure in atomic spectra [9.3], the test of quantum electrodynamics by precision measurements of the Lamb shift [9.4] or the still unresolved problem of a possible time dependence of physical fundamental constants, which might be solved by performing extremely accurate optical frequency measurements. In this chapter some of these new and exciting developments are presented.

9.1 Optical Cooling and Trapping of Atoms

In order to improve the accuracy of spectroscopic measurements of atomic energy levels, all perturbing effects leading to broadening or shifts of these levels must be either eliminated or should be sufficiently well understood to introduce appropriate corrections. One of the largest perturbing effects is the thermal motion of atoms. In Chap. 4 we saw that in collimated atomic beams the velocity components v_x and v_y, which are perpendicular to the beam axes, can be drastically reduced by collimating apertures (geometrical cooling). The component v_z can be compressed by adiabatic cooling into a small interval $v_z = u \pm \Delta v_z$ around the flow velocity u. If this reduction of the velocity distribution is described by a *translational temperature* T_{trans}, values of $T_{\text{trans}} < 1\,\text{K}$ can be reached. However, the molecules still have a nearly uniform but large velocity u, and broadening effects such as transit-time broadening or shifts caused by the second-order Doppler effect (see below) are not eliminated.

In this section we discuss the new technique of *optical cooling*, which decreases the velocity of atoms to a small interval around $v = 0$. Optical cooling down to "temperatures" of a few microKelvin has been achieved; by combining optical and evaporative cooling even the nanoKelvin range was reached.

This brought the discovery of quite new phenomena, such as Bose–Einstein condensation or atom–lasers, and atomic fountains. [9.5–9.7].

9.1.1 Photon Recoil

Let us consider an atom with rest mass M in the energy level E_i that moves with the velocity $\boldsymbol{v}$. If this atom absorbs a photon of energy $\hbar\omega_{ik} \simeq E_k - E_i$ and momentum $\hbar\boldsymbol{k}$, it is excited into the level E_k. Its momentum changes from $\boldsymbol{p}_i = M\boldsymbol{v}_i$ before the absorption to

$$\boldsymbol{p}_k = \boldsymbol{p}_i + \hbar\boldsymbol{k}\,, \tag{9.1}$$

after the absorption (the *recoil effect*, Fig. 9.1).

The relativistic energy conservation demands

$$\hbar\omega_{ik} = \sqrt{p_k^2c^2 + (M_0c^2 + E_k)^2} - \sqrt{p_i^2c^2 + (M_0c^2 + E_i)^2}\,. \tag{9.2}$$

When we extract $(M_0c^2 + E_k)$ from the first root and $(M_0c^2 + E_i)$ from the second, we obtain by a Taylor expansion the power series for the resonant absorption frequency

$$\omega_{ik} = \omega_0 + \boldsymbol{k}\cdot\boldsymbol{v}_i - \omega_0\frac{v_i^2}{2c^2} + \frac{\hbar\omega_0^2}{2Mc^2} + \ldots\,. \tag{9.3}$$

The first term represents the absorption frequency $\omega_0 = (E_k - E_i)$ of an atom at rest if the recoil of the absorbing atom is neglected. The second term describes the linear Doppler shift (first-order Doppler effect) caused by the motion of the atom at the time of absorption. The third term expresses the quadratic Doppler effect (second-order Doppler effect). Note that this term is independent of the direction of the velocity $\boldsymbol{v}$. It is therefore *not* eliminated by the "Doppler-free" techniques described in Chaps. 2–5, which only overcome the *linear* Doppler effect.

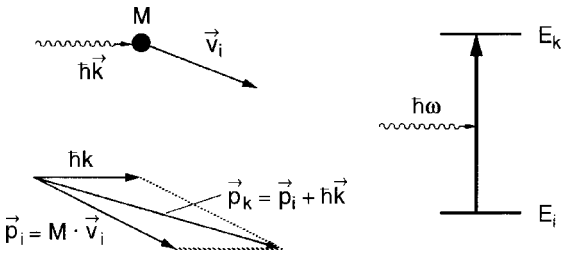

Fig. 9.1. Atomic recoil for absorption and emission of a photon

Example 9.1.
A parallel beam of Ne ions accelerated by 10 keV moves with the velocity $v_z = 3 \times 10^5$ m/s. When the beam is crossed perpendicularly by a single-mode laser beam tuned to a transition with $\lambda = 500$ nm, even ions with $v_x = v_y = 0$ show a quadratic relativistic Doppler shift of $\Delta\nu/\nu = 5 \times 10^{-7}$, which yields an absolute shift of $\Delta\nu = 250$ MHz. This should be compared with the linear Doppler shift of 600 GHz, which appears when the laser beam is parallel to the ion beam (Example 4.6).

The last term in (9.3) represents the recoil energy of the atom from momentum conservation. The energy $\hbar\omega$ of the absorbed photon has to be larger than that for recoil-free absorption by the amount

$$\Delta E = \frac{\hbar^2\omega_0^2}{2Mc^2} \quad \Rightarrow \quad \frac{\Delta E}{\hbar\omega} = \frac{1}{2}\frac{\hbar\omega}{Mc^2} \,. \tag{9.4}$$

When the excited atom in the state E_k with the momentum $\boldsymbol{p}_k = M\boldsymbol{v}_k$ emits a photon, its momentum changes to

$$\boldsymbol{p}_i = \boldsymbol{p}_k - \hbar\boldsymbol{k}$$

after the emission. The emission frequency becomes analogous to (9.3)

$$\omega_{ik} = \omega_0 + k\boldsymbol{v}_k - \frac{\omega_0 v_k^2}{2c^2} - \frac{\hbar\omega_0^2}{2Mc^2} \,. \tag{9.5}$$

The difference between the resonant absorption and emission frequencies is

$$\Delta\omega = \omega_{ik}^{\text{abs}} - \omega_{ki}^{\text{em}} = \frac{\hbar\omega_0^2}{Mc^2} + \frac{\omega_0}{2c^2}(v_k^2 - v_i^2) \approx \frac{\hbar\omega_0^2}{Mc^2} \,, \tag{9.6}$$

since the second term can be written as $(\omega_0/Mc^2)\cdot(E_k^{\text{kin}} - E_i^{\text{kin}})$ and $\Delta E^{\text{kin}} \ll \hbar\omega$. It can be therefore neglected for atoms with thermal velocities.

The relative frequency shift between absorbed and emitted photons because of recoil

$$\frac{\Delta\omega}{\omega} = \frac{\hbar\omega_0}{Mc^2} \,, \tag{9.7}$$

equals the ratio of photon energy to rest-mass energy of the atom.

For γ-quanta in the MeV range this ratio may be sufficiently large that $\Delta\omega$ becomes larger than the linewidth of the absorbing transition. This means that a γ-photon emitted from a free nucleus cannot be absorbed by another identical nucleus at rest. The recoil can be greatly reduced if the atoms are embedded in a rigid crystal structure below the Debye temperature. This recoil-free absorption and emission of γ-quanta is called the *Mössbauer effect* [9.8].

In the *optical region* the recoil shift $\Delta\omega$ is extremely small and well below the natural linewidth of most optical transitions. Nevertheless, it has been measured for selected narrow transitions [9.9, 9.10].

9.1.2 Measurement of Recoil Shift

When the absorbing molecules with the resonant absorption frequency ω_0 are placed inside the laser resonator, the standing laser wave of frequency $\omega \neq \omega_0$ burns two Bennet holes into the population distribution $N_i(v_z)$ (Fig. 9.2b and Sect. 2.2), which, according to (9.3), appear at the velocity components

$$v_{zi} = \pm[\omega' - \hbar\omega_0^2/(2Mc^2)]/k\,, \quad \text{with} \quad \omega' = \omega - \omega_0(1 - v^2/2c^2)\,. \tag{9.8}$$

The corresponding peaks in the population distribution $N_k(v_z)$ of molecules in the upper level $|k\rangle$ are shifted due to photon recoil (Fig. 9.2a). They show up, according to (9.5), at the velocity components

$$v_{zk} = \pm[\omega' + \hbar\omega_0^2/(2Mc^2)]/k\,. \tag{9.9}$$

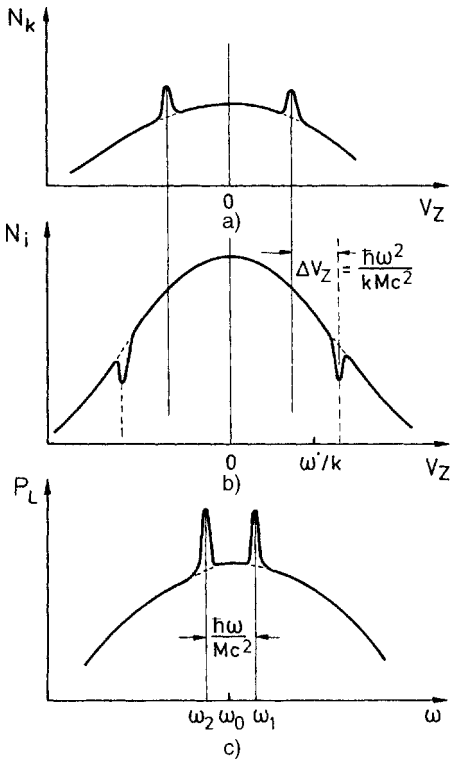

Fig. 9.2a–c. Generation of the recoil doublet of Lamb dips: (**a**) population peaks in the upper-state population for $\omega \neq \omega_0$; (**b**) Bennet holes in the lower-state population; (**c**)recoil doublet in the output power $P_L(\omega)$ of the laser

For the example, illustrated by Fig. 9.2, we have chosen

$$\omega < \omega_0 \;\Rightarrow\; \omega' < 0\,.$$

The two holes in the ground-state population coincide for $v_{zi} = 0$, which gives $\omega' = \hbar\omega_0^2/2Mc^2$. This happens, according to (9.8), for the laser frequency

$$\omega = \omega_1 = \omega_0[(1 - v^2/c^2) + \hbar\omega_0/(2Mc^2)]\,, \tag{9.10a}$$

while the two peaks in the upper level population coincide for another laser frequency

$$\omega = \omega_2 = \omega_0[(1 - v^2/c^2) - \hbar\omega_0/(2Mc^2)]\,. \tag{9.10b}$$

The absorption of the laser is proportional to the population difference $\Delta N = N_i - N_k$. This difference has two maxima at ω_1 and ω_2. The laser output therefore exhibits two Lamb peaks (*inverse Lamb dips*) (Fig. 9.2c) at the laser frequencies ω_1 and ω_2, which are separated by twice the recoil energy

$$\Delta\omega = \omega_1 - \omega_2 = \hbar\omega^2/Mc^2\,. \tag{9.11}$$

Example 9.2.

(a) For the transition at $\lambda = 3.39\,\mu\text{m}$ in the CH_4 molecule ($M = 16\,\text{AMU}$) the recoil splitting amounts to $\Delta\omega = 2\pi \cdot 2.16\,\text{kHz}$, which is still larger than the natural linewidth of this transition [9.10, 9.11].
(b) For the calcium intercombination line $^1S_0 \rightarrow {}^3P_1$ at $\lambda = 657\,\text{nm}$ we obtain with $M = 40\,\text{AMU}$ the splitting $\Delta\omega = 2\pi \cdot 23.1\,\text{kHz}$ [9.12].
(c) For a rotation–vibration transition in SF_6 at $\lambda = 10\,\mu\text{m}$ the frequency ω is one-third that of CH_4 but the mass 10 times larger than for CH_4. The recoil splitting therefore amounts only to about 0.02 kHz and is not measurable [9.14]

Since such small splittings can only be observed if the width of the Lamb peaks is smaller than the recoil shift, all possible broadening effects, such as pressure broadening and transit-time broadening, must be carefully minimized. This can be achieved in experiments at low pressures and with expanded laser beam diameters [9.13]. An experimental example is displayed in Fig. 9.3.

The velocities of very cold atoms are very small, i.e., the linear and the quadratic Doppler effects both become small and the recoil term becomes significant. It turns out that for cold Ca atoms at $T = 10\,\mu\text{K}$, the recoil effect leads to large asymmetries in the Lamb dips of absorption spectra taken with short pulses [9.15]. These are not found in experiments performed at room temperature, where the broad Doppler background masks these asymmetries, and they are based on the fundamental asymmetry between absorption and stimulated emission with short pulses.

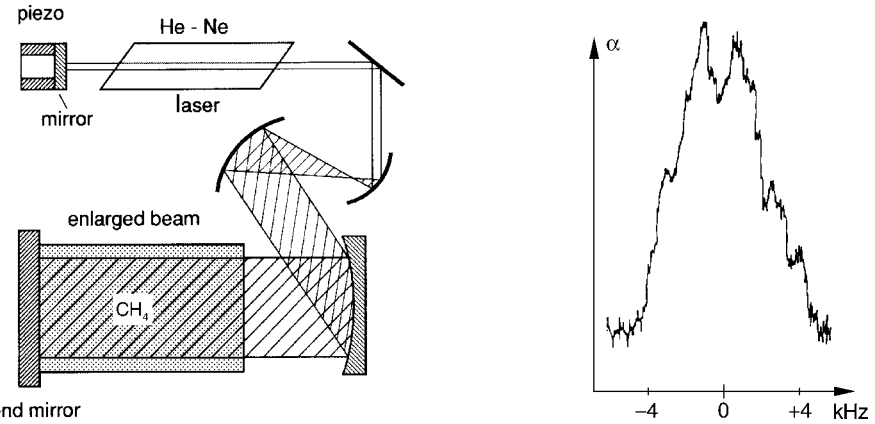

Fig. 9.3. Schematic experimental arrangement for measuring the recoil splitting and the measured signal of the recoil doublet of the hyperfine component $8 \rightarrow 7$ of the $(P(7), \nu_3)$ transition at $\lambda = 3.39\,\mu m$ in methane [9.11]

The transit-time broadening can greatly be reduced by the optical Ramsey method of separated fields. The best resolution of the recoil splittings has indeed been achieved with this technique (Sect. 9.4). The transit time can also be increased if only molecules with small transverse velocity components contribute to the Lamb dip. If the laser intensity is kept so small that saturation of the molecular transition is reached only for molecules that stay within the laser beam for a sufficiently long time, that is, molecules with small components v_x, v_y, the transit-time broadening is greatly reduced [9.11].

9.1.3 Optical Cooling by Photon Recoil

Although the recoil effect is very small when a single photon is absorbed, it can be used effectively for optical cooling of atoms by the cumulative effect of many absorbed photons. This can be seen as follows:

When atom A stays for the time T in a laser field that is in resonance with the transition $|i\rangle \rightarrow |k\rangle$, the atom may absorb and emit a photon $\hbar\omega$ many times, provided the optical pumping cycle is short compared to T and the atom behaves like a true two-level system. This means that the emission of fluorescence photons $\hbar\omega$ by the excited atom in level $|k\rangle$ brings the atom back only to the initial state $|i\rangle$, but never to other levels. With the saturation parameter $S = B_{ik}\rho(\omega_{ik})/A_{ik}$, the fraction of excited atoms becomes

$$\frac{N_k}{N} = \frac{S}{1+2S} .$$

The fluorescence rate is $N_k A_k = N_k/\tau_k$. Since N_k can never exceed the saturated value $N_k = (N_i + N_k)/2 = N/2$, the minimum recycling time for the saturation parameter $S \rightarrow \infty$ (Sect. 3.6) is $\Delta T = 2\tau_k$.

Example 9.3.

When an atom passes with a thermal velocity $v = 500\,\mathrm{m/s}$ through a laser beam with 2-mm diameter, the transit time is $T = 4\,\mu\mathrm{s}$. For a spontaneous lifetime $\tau_k = 10^{-8}\,\mathrm{s}$ the atom can undergo $q \leq (T/2)/\tau_k = 400$ absorption–emission cycles during its transit time.

When a laser beam is sent through a sample of absorbing atoms, the LIF is generally isotropic, that is, the spontaneously emitted photons are randomly distributed over all spatial directions. Although each emitted photon transfers the momentum $\hbar\boldsymbol{k}$ to the emitting atoms, the time-averaged momentum transfer tends to zero for sufficiently large values of $q = T/2\tau_k$.

The *absorbed* photons, however, all come from the same direction. Therefore, the momentum transfer for q absorptions adds up to a total recoil momentum $\boldsymbol{p} = q\hbar\boldsymbol{k}$ (Fig. 9.4). This changes the velocity $\boldsymbol{v}$ of an atom which flies against the beam propagation by the amount $\Delta v = \hbar k/M$ per absorption. For q absorption–emission cycles we get

$$\Delta v = q\frac{\hbar k}{M} = q\frac{\hbar\omega}{Mc}\,. \tag{9.12a}$$

Atoms in a collimated atomic beam can therefore be slowed down by a laser beam propagating anticollinearly to the atomic beam [9.16]. This can be expressed by the "cooling force"

$$\boldsymbol{F} = M\frac{\Delta\boldsymbol{v}}{\Delta T} = \frac{\hbar\boldsymbol{k}}{\tau_k}\frac{S}{1+2S}\,. \tag{9.12b}$$

Note that the *recoil energy* transferred to the atom

$$\Delta E_{\mathrm{recoil}} = q\frac{\hbar^2\omega^2}{2Mc^2}\,, \tag{9.13}$$

is still very small.

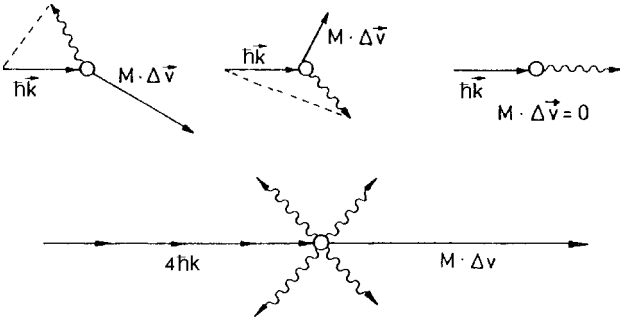

Fig. 9.4. Recoil momentum of an atom for a fixed direction of the absorbed photons but different directions of the emitted fluorescence photons

Example 9.4.

(a) For Na atoms with $M = 23$ AMU, which absorb photons $\hbar\omega \simeq 2$ eV on the transition $3\,^2S_{1/2} \rightarrow 3\,^2P_{3/2}$, (9.12) gives $\Delta v = 3$ cm/s per photon absorption. In order to reduce the initial thermal velocity of $v = 600$ m/s at $T = 500$ K to 20 m/s (this would correspond to a temperature $T = 0.6$ K for a thermal distribution with $\overline{v} = 20$ m/s),this demands $q = 2 \times 10^4$ absorption–emission cycles. At the spontaneous lifetime $\tau_k = 16$ ns a minimum cooling time of $T = 2 \times 10^4 \cdot 2 \cdot 16 \times 10^{-9}$ s $\simeq 600\,\mu$s is required. This gives a negative acceleration of $a = -10^6$ m/s^2, which is 10^5 times the gravity acceleration on earth $g = 9.81$ m/s^2! During the time T the atom has traveled the distance $\Delta_z = v_0 T - \frac{1}{2} a T^2 \simeq 18$ cm. During this deceleration path length it always has to remain within the laser beam. The total energy transferred by recoil to the atom is only -2×10^{-2} eV. It corresponds to the kinetic energy $\frac{1}{2} M v^2$ of the atom and is very small compared to $\hbar\omega = 2$ eV.

(b) For Mg atoms with $M = 24$ AMU, which absorb on the singlet resonance transition at $\lambda = 285.2$ nm, the situation is more favorable because of the higher photon energy $\hbar\omega \simeq 3.7$ eV and the shorter lifetime $\tau_k = 2$ ns of the upper level. One obtains: $\Delta v = -6$ cm/s per absorbed photon; $q = 1.3 \times 10^4$. The minimum cooling time becomes $T = 3 \times 10^{-5}$ s and the deceleration path length $\Delta z \simeq 1$ cm.

(c) In [9.17] a list of other atoms can be found that were regarded as possible candidates for optical cooling. Some of them have since been successfully tried.

The following remarks may be useful:

(a) Without additional tricks, this optical-cooling method is restricted to true two-level systems. Therefore, *molecules cannot be cooled with this technique*, because after their excitation into level $|k\rangle$ they return by emission of fluorescence into many lower vibrational–rotational levels and only a small fraction goes back into the initial level $|i\rangle$. Thus, only one optical pumping cycle is possible. There have been, however, other cooling mechanisms for molecules proposed and partly realized (see Sect. 9.1.5).

(b) The sodium transition $3S - 3P$, which represents the standard example for optical cooling, is in fact a multi level system because of its hyperfine structure (Fig. 9.5). However, after optical pumping with circularly polarized light on the hfs transition $3\,^2S_{1/2}(F'' = 2) \rightarrow 3\,^2P_{3/2}(F' = 3)$, the fluorescence can only reach the initial lower level $F'' = 2$. A true two-level system would be realized if any overlap of the pump transition with other hfs components could be avoided (see below).

(c) Increasing the intensity of the pump laser decreases the time ΔT for an absorption–emission cycle. However, for saturation parameters $S > 1$ this decrease is small and ΔT soon reaches its limit $2\tau_k$. On the other hand, the induced emission increases at the expense of spontaneous emission.

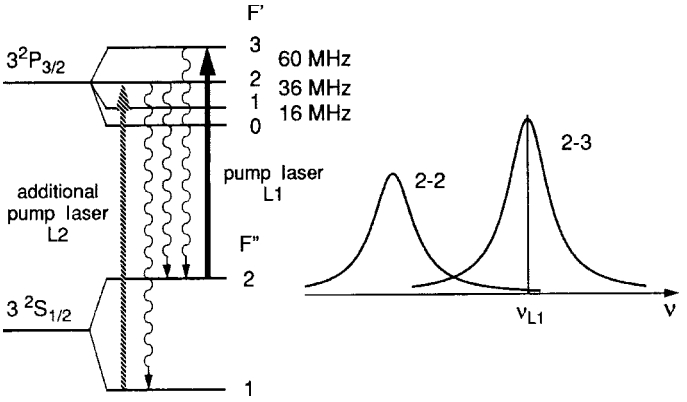

Fig. 9.5. Level diagram of the Na $3\,^2S_{1/2} \rightarrow 3\,^2P_{3/2}$ transition with hyperfine splittings. Optical pumping on the hfs component $F'' = 2 \rightarrow F' = 3$ represents a true two-level system, provided any overlap between the hfs components can be avoided. The additional pump laser L2 is necessary in order to pump atoms tranferred into level $F'' = 1$ by spectral overlap between the components $2 \rightarrow 3$ and $2 \rightarrow 2$ back into level $F'' = 2$

Since the emitted induced photon has the same $\boldsymbol{k}$-vector as the absorbed induced photon, the net momentum transfer is zero. The total deceleration rate therefore has a maximum at the optimum saturation parameter $S \simeq 1$.

9.1.4 Experimental Arrangements

For the experimental realization of optical cooling, which uses a collimated beam of atoms and a counterpropagating cw laser (dye laser or diode laser, Fig. 9.6) the following difficulties have to be overcome: during the decelera-

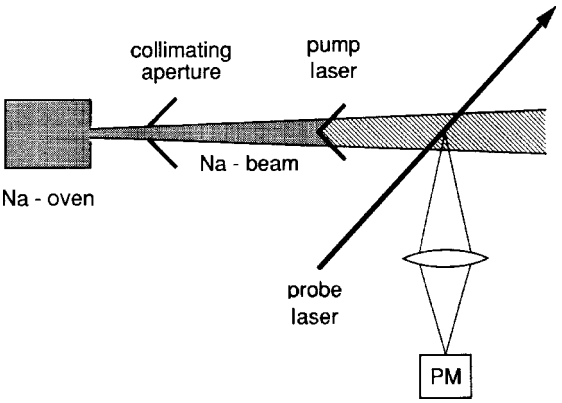

Fig. 9.6. Simplified experimental realization for the deceleration of atoms in a collimated beam by photon recoil

tion time the Doppler-shifted absorption frequency $\omega(t) = \omega_0 + \boldsymbol{k} \cdot \boldsymbol{v}(t)$ changes with the decreasing velocity v, and the atoms would come out of resonance with the monochromatic laser. Three solutions have been successfully tried: either the laser frequency

$$\omega(t) = \omega_0 + k \cdot v(t) \pm \gamma \,, \tag{9.14}$$

is synchronously tuned with the changing velocity $v(t)$ in order to stay within the linewidth γ of the atomic transition [9.18, 9.19], or the absorption frequency of the atom is appropriately altered along the deceleration path [9.20, 9.21]. A third alternative uses a broadband laser for cooling. We will discuss these methods briefly:

When the laser frequency ω for a counterpropagating beam $\boldsymbol{k}$ antiparallel to $\boldsymbol{v}$ is kept in resonance with the constant atomic frequency ω_0, it must have the time dependence

$$\omega(t) = \omega_0 \left(1 - \frac{v(t)}{c}\right) \quad \Rightarrow \quad \frac{\mathrm{d}\omega}{\mathrm{d}t} = -\frac{\omega_0}{c}\frac{\mathrm{d}v}{\mathrm{d}t} \,. \tag{9.15}$$

The velocity change per second for the optimum deceleration with a pump cycle period $T = 2\tau$ is, according to (9.12)

$$\frac{\mathrm{d}v}{\mathrm{d}t} = \frac{\hbar\omega_0}{2Mc\tau} \,. \tag{9.16}$$

Inserting this into (9.15) yields for the necessary time dependence of the laser frequency

$$\omega_\mathrm{L}(t) = \omega(0)(1 + \alpha t) \,, \quad \text{with} \quad \alpha = \frac{\hbar\omega_0}{2Mc^2\tau} \ll 1 \,. \tag{9.17}$$

This means that the pump laser should have a linear frequency chirp.

Example 9.5.

For Na atoms with $v(0) = 1000\,\mathrm{m/s}$, insertion of the relevant numbers into (9.17) yields $\mathrm{d}\omega/\mathrm{d}t = 2\pi \cdot 1.7\,\mathrm{GHz/ms}$, which means that fast frequency tuning in a controlled way is required in order to fulfill (9.17).

An experimental realization of the controlled frequency chirp uses amplitude modulation of the laser with the modulation frequency Ω_1. The sideband at $\omega_\mathrm{L} - \Omega_1$ is tuned to the atomic transition and can be matched to the time-dependent Doppler shift by changing $\Omega_1(t)$ in time. In order to compensate for optical pumping into other levels than $F'' = 2$ by overlap of the laser with other hfs components, the transition $F'' = 1 \rightarrow F' = 2$ is simultaneously pumped (Fig. 9.5). This can be achieved if the pump laser is additionally modulated at the second frequency Ω_2, where the sideband $\omega_\mathrm{L} + \Omega_2$ matches the transition $F'' = 1 \rightarrow F' = 2$ [9.19, 9.22].

For the second method, where the laser frequency ω_L is kept constant, the atomic absorption frequency must be altered during the deceleration of the atoms. This can be realized by Zeeman tuning (Fig. 9.7). In order to match the

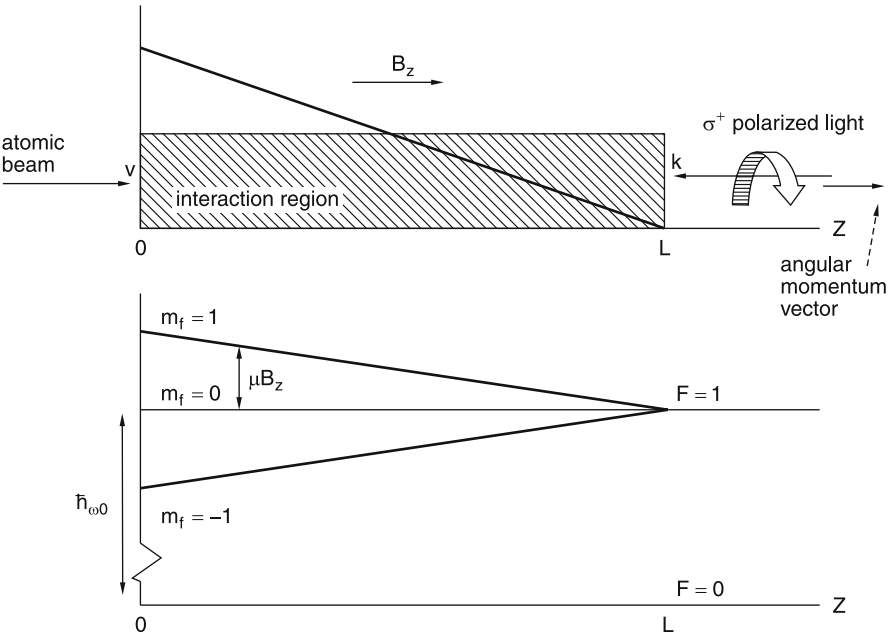

Fig. 9.7. Level diagram for laser cooling by Zeeman tuning

Zeeman shift to the changing Doppler shift $\Delta\omega(z)$, the longitudinal magnetic field must have the z-dependence

$$B = B_0\sqrt{1-2az/v_0^2}\,, \tag{9.18}$$

for atoms that enter the field at $z = 0$ with the velocity v_0 and experience the negative acceleration a [m/s^2] by photon recoil [9.21]. This field dependence $B(z)$ can be realized by a proper choice of the windings $N_W(z)$ per centimeters of the magnetic field coil (Fig. 9.8)

Most optical cooling experiments have been performed up to now on alkali atoms, such as Na or Rb, using a single-mode cw dye laser. The velocity decrease of the atoms is monitored with the tunable probe laser L2, which is sufficiently weak that it does not affect the velocity distribution. The probe-laser-induced fluorescence $I_{Fl}(\omega_2)$ is measured as a function of the Doppler shift. Experiments have shown that the atoms could be completely stopped and their velocity could even be reversed [9.18]. An example of the compression of the thermal velocity distribution into a narrow range around $v = 200\,\mathrm{m/s}$ is illustrated in Fig. 9.9 for Na atoms.

A favorable alternative to dye lasers is a GaAs diode laser, which can cool rubidium or cesium atoms [9.23–9.25] and also metastable noble gas atoms, such as He* or Ar* [9.26]. The experimental expenditures are greatly reduced since the GaAs laser is much less expensive than an argon laser plus dye-laser combination. Furthermore, the frequency modulation is more readily realized with a diode laser than with a dye laser.

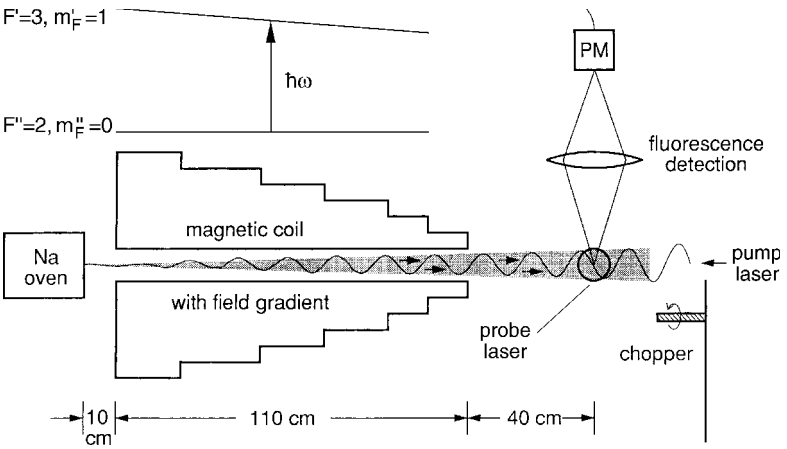

Fig. 9.8. Laser cooling of atoms in a collimated beam with a fixed laser frequency and Zeeman tuning of the atomic absorption frequency [9.21]

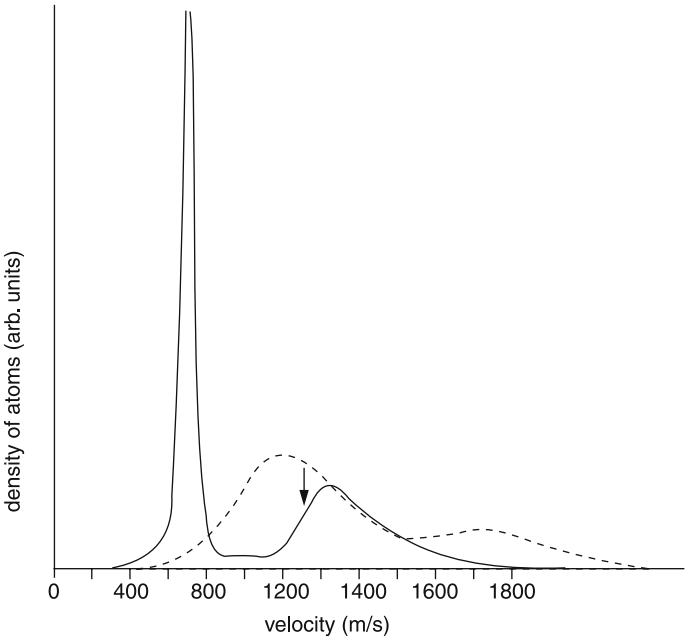

Fig. 9.9. Velocity distribution before (*dashed*) and after (*solid*) Zeeman cooling. The *arrow* indicates the highest velocity resonant with the slowing laser. (The extra bump at 1700 m/s is from $F = 1$ atoms, which are optically pumped into $F = 2$ during the cooling process) [W. Phillips, Nobel Lecture 1995]

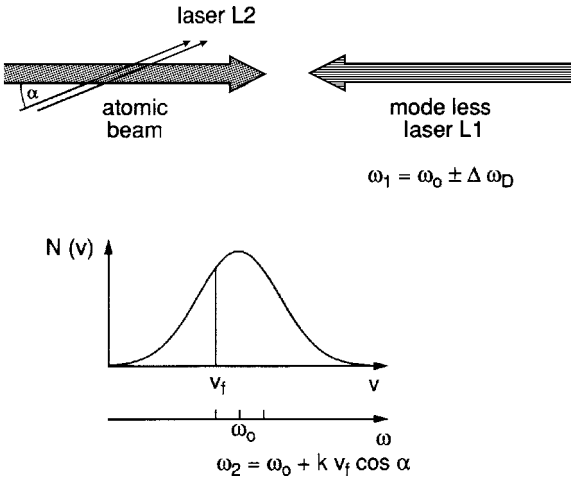

Fig. 9.10. Cooling of all atoms with a counterpropagating modeless laser. A cooling stop at a selectable velocity v_f can be realized with a second copropagating single-mode laser [9.29]

A very interesting alternative laser for optical cooling of atoms in a collimated beam is the *modeless* laser [9.27], which has a broad spectral emission (without mode structure, when averaged over a time of $T > 10$ ns, with an adjustable bandwidth and a tunable center frequency). Such a laser can cool all atoms regardless of their velocity if its spectral width $\Delta\omega_L$ is larger than the Doppler shift $\Delta\omega_D = v_0 k$ [9.28].

With the following experimental trick it is possible to compress the velocity distribution $N(v_z)$ of atoms in a beam into a small interval Δv_z around a wanted final velocity v_f. The beam from the modeless laser propagates anticollinearly to the atomic beam and cools the atoms (Fig. 9.10). A second single-mode laser intersects the atomic beam under a small angle α against the beam axis. If it is tuned to the frequency

$$\omega_2 = \omega_0 + k v_f \cos\alpha \,,$$

it accelerates the atoms as soon as they have reached the velocity v_f. This second laser therefore acts as a barrier for the lower velocity limit of cooled atoms [9.29].

The photon recoil can be used not only for the deceleration of collimated atomic beams but also for the deflection of the atoms, if the laser beam crosses the atomic beam perpendicularly [9.30–9.32]. In order to increase the transferred photon momentum, and with it the deflection angle, an experimental arrangement is chosen where the laser beam crosses the atomic beam many times in the same direction (Fig. 9.11). The deflection angle δ per absorbed photon, which is given by $\tan\delta = \hbar k/(m v_z)$, increases with decreasing atomic velocity v_z. Optically cooled atoms can therefore be deflected by large angles. Since the atomic absorption frequency differs for different isotopes, this

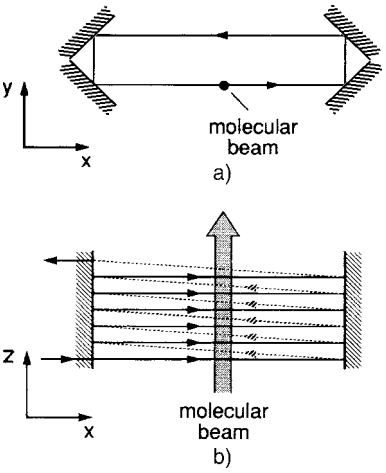

Fig. 9.11. Deflection of atoms in a collimated atomic beam using a multiple-path geometry. The molecular beam travels into the z-direction: (**a**) view into the z-direction; (**b**) view into the y-direction. On the *dashed* return paths the laser beam does not intersect the atomic beam

deflection can be used for spatial isotope separation [9.33] if other methods cannot be applied (Sect. 10.1.6).

An interesting application of atomic deflection by photon recoil is the collimation and focusing of atomic beams with lasers [9.34]. Assume atoms with the velocity $\boldsymbol{v} = \{v_x \ll v_z, 0, v_z\}$ pass through a laser resonator, where an intense standing optical wave in the $\pm x$-direction is present. If the laser frequency ω_L is kept slightly below the atomic resonance frequency ω_0 ($\gamma > \omega_0 - \omega_\mathrm{L} > 0$), atoms with transverse velocity components v_x are always pushed back to the z-axis by photon recoil because that part of the laser wave with the $\boldsymbol{k}$-vector antiparallel to v_x always has a larger absorption probabil-

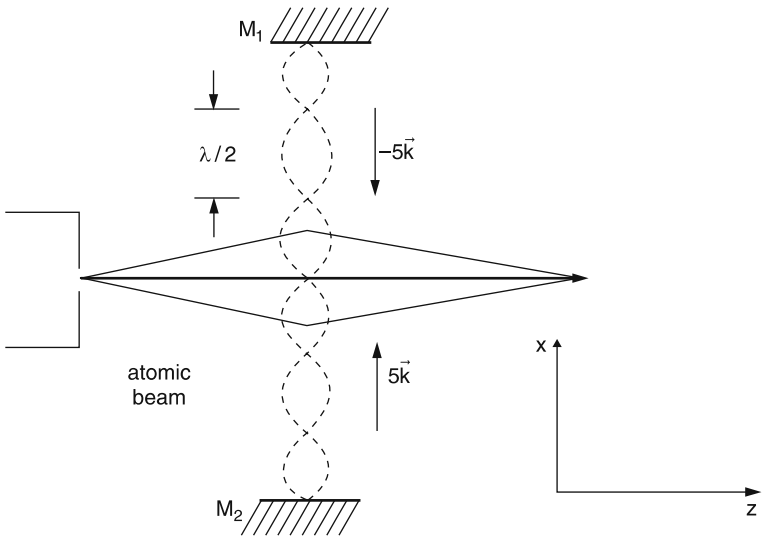

Fig. 9.12. Standing optical wave acting as a lens for a divergent atomic beam

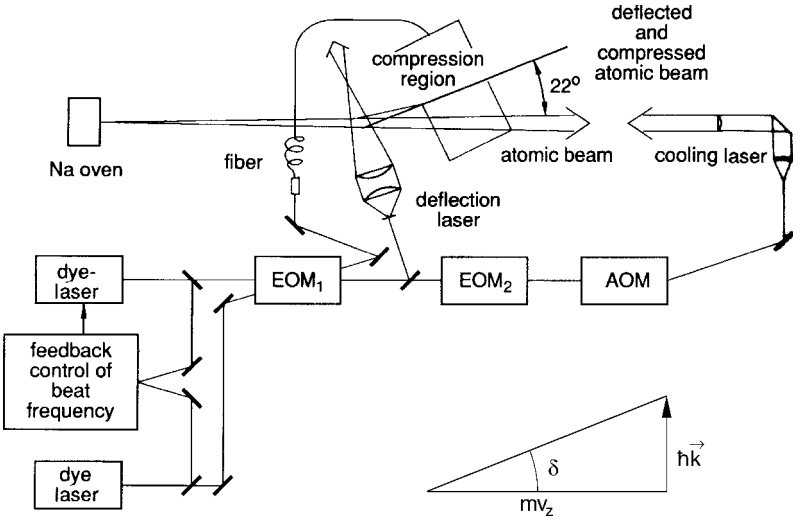

Fig. 9.13. Cooling, deflection and compression of atoms by photon recoil. The electro-optic modulators (EOM) and the acousto-optic modulator (AOM) serve for sideband generation and frequency tuning of the cooling laser sideband [9.32]

ity than the component with $\boldsymbol{k}$ parallel to v_x. The velocity component v_x is therefore reduced and the atomic beam is collimated.

If the atoms have been optically cooled before they pass the standing laser wave, they experience a large collimation in the maximum of the standing wave, but are not affected in the nodes. The laser wave acts like a transmission grating that "channels" the transmitted atoms and focuses the different channels (Fig. 9.12) [9.35].

A schematic diagram of an apparatus for optical cooling of atoms, deflection of the slowed-down atoms, and focusing is depicted in Fig. 9.13.

9.1.5 Threedimensional Cooling of Atoms; Optical Mollasses

Up to now we have only considered the cooling of atoms that all move into one direction. Therefore only one velocity component has been reduced by photon recoil. For cooling of atoms in a thermal gas where all three velocity components $\pm v_x$, $\pm v_y$, $\pm v_z$ have to be reduced, six laser beams propagating into the $\pm x$-, $\pm y$-, $\pm z$-directions are required [9.36]. All six beams are generated by splitting a single laser beam (Fig. 9.14). If the laser frequency is tuned to the red side of the atomic resonance ($\Delta\omega = \omega - \omega_0 < 0$), a repulsive force is always acting on the atoms, because for atoms moving toward the laser wave ($\boldsymbol{k} \cdot \boldsymbol{v} < 0$) the Doppler-shifted absorption frequency is shifted toward the resonance frequency ω_0, whereas for the counterpropagating wave ($\boldsymbol{k} \cdot \boldsymbol{v} > 0$) it is shifted away from resonance (Fig. 9.15). For a quantitative description we denote the absorption rate $R \propto \sigma(\omega)$ of an atom with $\boldsymbol{k} \cdot \boldsymbol{v} > 0$ by $R^+(v)$, and

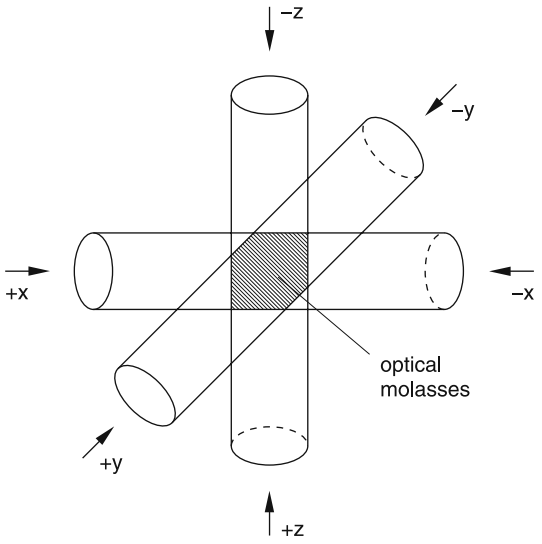

Fig. 9.14. Optical molasses with six pairwise counterpropagating laser beams

for $\boldsymbol{k}\cdot\boldsymbol{v}<0$ by $R^{-}(v)$. The net recoil force component F_i $(i=x,y,z)$ is then

$$F_i=[R^{+}(v_i)-R^{-}(v_i)]\cdot\hbar k\,. \tag{9.19}$$

For a Lorentzian absorption profile with FHWM γ, the frequency dependence of the absorption rate is (Fig. 9.15)

$$R^{\pm}(v)=\frac{R_0}{1+\left(\dfrac{\omega_{\mathrm{L}}-\omega_0\mp kv}{\gamma/2}\right)^2}\,. \tag{9.20}$$

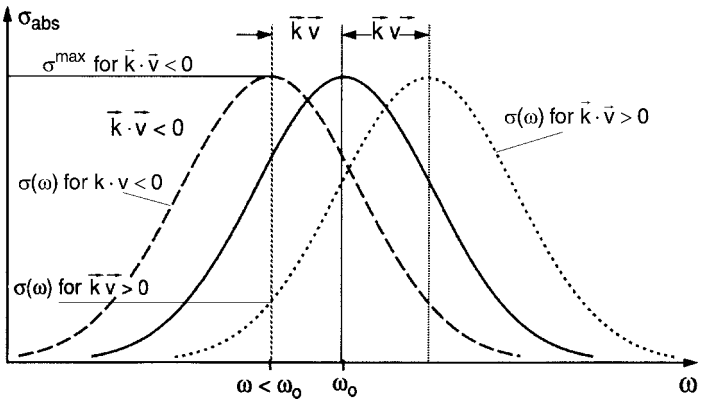

Fig. 9.15. For $\omega<\omega_0$, the absorption probability is larger for $\boldsymbol{k}\cdot\boldsymbol{v}<0$ than for $\boldsymbol{k}\cdot\boldsymbol{v}>0$

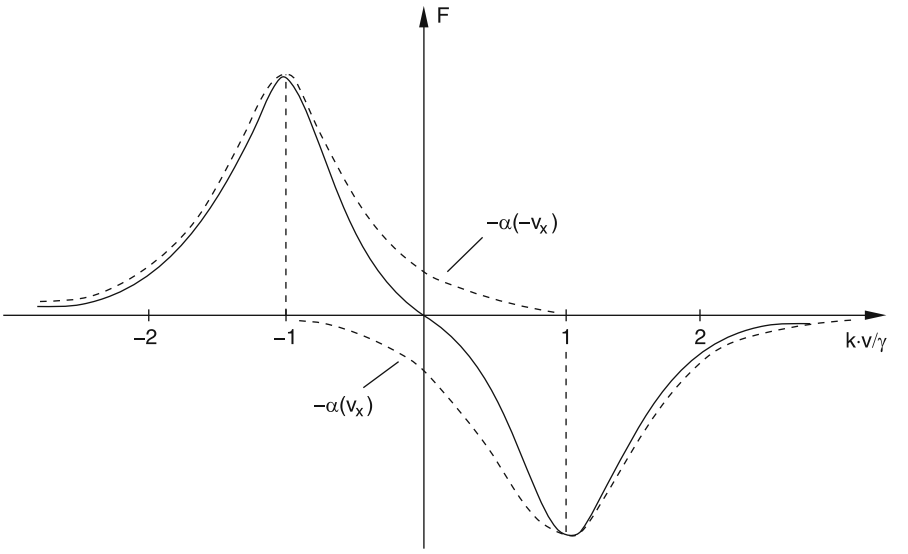

Fig. 9.16. Frictional force in an optical molasses (*solid curve*) for a red detuning $\delta = -\gamma$. The *dotted curve* shows the absorption profiles by a single atom moving with $v_x = \pm\gamma/k$ for a single laser beam propagating into the x-direction

Inserting (9.20) into (9.19) yields for $\boldsymbol{k}\cdot\boldsymbol{v} \ll \omega_{\mathrm{L}} - \omega_0 = \delta$ the net force (Fig. 9.16)

$$F_i = -a\cdot v_i\,, \quad \text{with} \quad a = R_0 \frac{16\delta\hbar k^2}{\gamma^2\left[1+(2\delta/\gamma)^2\right]^2}\,. \tag{9.21}$$

An atom moving within the overlap region of the six running laser waves therefore experiences a force $F_i(v_i) = -av_i$ $(i = x, y, z)$ that damps its velocity. From the relation $\mathrm{d}v/\mathrm{d}t = F/m \Rightarrow \mathrm{d}v/v = -a/m\,\mathrm{d}t$ we obtain the time-dependent velocity

$$v = v_0\,\mathrm{e}^{-(a/m)t}\,. \tag{9.22}$$

The velocity decreases exponentially with a damping time $t_{\mathrm{D}} = m/a$.

Example 9.6.

(a) For rubidium atoms ($m = 85$ AMU) the wavenumber is $k = 8\times10^6\,\mathrm{m}^{-1}$. At a detuning $\delta = \gamma$ and an absorption rate $R_0 = \gamma/2$ we obtain: $a = 4\times10^{-21}\,\mathrm{Ns/m}$. This gives a damping time $t = 35\,\mu\mathrm{s}$.

(b) For Na atoms with $\delta = 2\gamma$ one obtains $a = 1\times10^{-20}\,\mathrm{Ns/m}$ and $t_{\mathrm{D}} = 2.3\,\mu\mathrm{s}$. The atoms move in this light trap like particles in viscous molasses and therefore this atomic trapping arrangement is often called *optical molasses*.

Note: These optical trapping methods reduce the velocity components (v_x, v_y, v_z) to a small interval around $v = 0$. However, they do *not* compress the atoms into a spatial volume, except if the dispersion force for the field gradients $\nabla I \neq 0$ is sufficiently strong. This can be achieved by electric or magnetic field gradients, as discussed in Sect. 9.1.7.

9.1.6 Cooling of Molecules

The optical cooling techniques discussed so far are restricted to true two-level systems because the cooling cycle of induced absorption and spontaneous emission has to be performed many times before the atoms come to rest. In molecules the fluorescence from the upper excited level generally ends in many rotational–vibrational levels in the electronic ground state that differ from the initial level. Therefore most of the molecules cannot be excited again with the same laser. They are lost for further cooling cycles.

Cold molecules are very interesting for several scientific and technical applications. One example is chemical reactions initiated by collisions between cold molecules where the collision time is very long and the reaction probability might become larger by several orders of magnitude. In addition, interactions of cold molecules with surfaces where the sticking coefficient will be 100% open up new insights into molecule–surface interactions and reactions between cold adsorbed molecules. Finally, the possibility to reach Bose–Einstein condensation of molecular gases opens new fascinating aspects of collective molecular quantum phenomena.

There have been several proposals how molecules might be cooled in spite of the above-mentioned difficulties [9.37–9.39]. An optical version of these proposals is based on a frequency comb laser, which oscillates on many frequencies, matching the relevant frequencies of the transitions from the upper to the lower levels with the highest transition probabilities [9.39]. In this case, the molecules can be repumped into the upper level from many lower levels, thus allowing at least several pumping cycles.

A very interesting optical cooling technique starts with the selective excitation of a collision pair of cold atoms into a bound level in an upper electronic state (Fig. 9.17). While this excitation occurs at the outer turning point of the upper-state potential, a second laser dumps the excited molecule down into a low vibrational level of the electronic ground state by stimulated emission pumping (photo-induced association). In favorable cases the level $v = 0$ can be reached. If the colliding atoms are sufficiently cold, the angular momentum of their relative movement is zero (S-wave scattering). Therefore the final ground state has the rotational quantum number $J = 0$ if the two lasers transfer no angular momentum to the molecule (either two transitions with $\Delta J = 0$ or the absorbing and emission transition as R-transitions with $\Delta J = +1$ in absorption and -1 in emission) [9.40]. The kinetic energy of the molecule formed by photoassociation is always smaller than that of the colliding atoms because of momentum conservation [5.116].

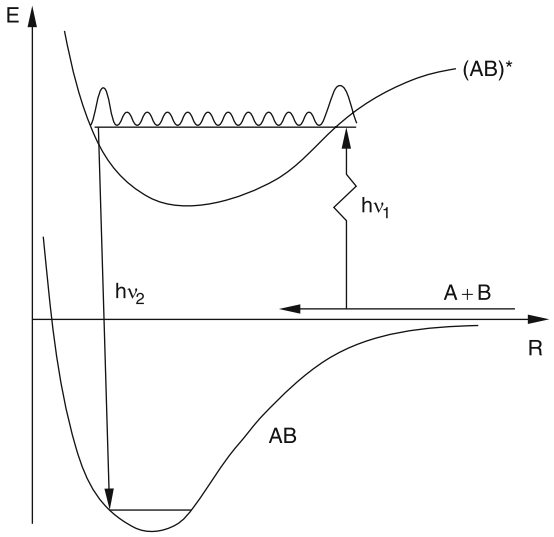

Fig. 9.17. Formation of cold molecules by photoassociation of a collision pair A+B

A promising nonoptical technique relies on cooling of molecules by collisions with cold atoms. If the gas mixture of atoms and molecules can be trapped in a sufficiently small volume long enough to achieve thermal equilibrium between atoms and molecules, the optically cooled atoms act as a heat sink for the molecules, which will approach the same temperature as the atoms (sympathetic cooling) [9.41].

An interesting proposal that could be realized uses a cold supersonic molecular beam with flow velocity u, which expands through a rotating nozzle (Fig. 9.18). We saw in Chap. 4 that in supersonic beams the velocity spread around the flow velocity u may become very small. The translational temperature in the frame moving with the velocity u can be as small as 0.1 K. If the nozzle moves with the speed $-v$, the molecules have the velocity $u - v$ in the laboratory frame. Tuning the angular velocity ω of the nozzle rotating on a circle with radius R makes it possible to reach any molecular velocity $v_m = u - \omega R$ between u and 0 in the laboratory frame. Since the beam must be collimated in order to reduce the other velocity components, there is only a small time interval per rotation period where the nozzle is in line with the collimating apertures. The cold molecules therefore appear as pulses behind the apertures.

An elegant technique has been developed in several laboratories, where cold helium clusters moving through a gas cell of atoms or molecules pick up these molecules, which then can diffuse into the interior of the helium cluster. The molecules then aquire the low temperature of the cluster. The binding energy is taken away by evaporation of He atoms from the cluster surface [9.42, 9.43].

At sufficiently low temperatures, the He droplet becomes superfluid [9.42]. The molecules inside the droplet can then freely rotate. Because the superfluid He droplet represents a quantum fluid with discrete excitation energies, the

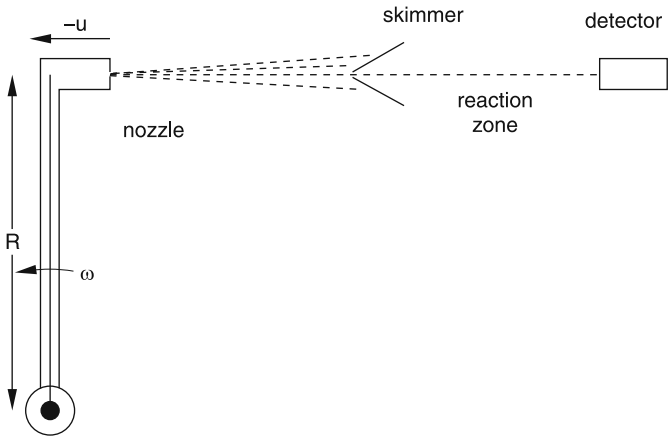

Fig. 9.18. Rotating nozzle for producing a beam of slow molecules

energy transfer between the molecule and its superfluid surroundings is limited and the molecular spectra show sharp lines. At the critical temperature between normal fluidity and superfluidity, the lines start to become broader. Laser spectroscopy of these molecules therefore gives direct information on the interaction of molecules and surroundings under different conditions from measured differences between the rotational spectrum of a free molecule and that for a molecule inside a cold He droplet. This has been verified for instance by M. Havenith and her group [9.42, 9.43].

Injecting different molecules into the He droplet gives the possibility to study chemical reactions between very cold molecules.

9.1.7 Optical Trapping of Atoms

The effectiveness of the optical molasses for cooling atoms anticipates that the atoms are trapped within the overlap region of the six laser beams for a sufficiently long time. This demands that the potential energy of the atoms shows a sufficiently deep minimum at the center of the trapping volume, that is, restoring forces must be present that will bring escaping atoms back to the center of the trapping volume.

We will briefly discuss the two most commonly used trapping arrangements. The first is based on induced electric dipole forces in inhomogeneous electric fields and the second on magnetic dipole forces in magnetic quadrupole fields. Letokhov proposed [9.46, 9.47] to use the potential minima of a three-dimensional standing optical field composed by the superposition of three perpendicular standing waves for spatial trapping of cooled atoms. It turns out that atoms can be indeed trapped this way, but only after they have been cooled down to very low temperatures. However, Ashkin and Gordon calculated [9.48] that the dispersion forces in focused Gaussian beams could be employed for trapping atoms.

a) Induced Dipole Forces in a Radiation Field

When an atom with the polarizability α is brought into an inhomogeneous electric field $\boldsymbol{E}$, a dipole moment $\boldsymbol{p} = \alpha \boldsymbol{E}$ is induced and the force

$$\boldsymbol{F} = -(\boldsymbol{p} \cdot \text{grad})\boldsymbol{E} = -\alpha(\boldsymbol{E} \cdot \nabla)\boldsymbol{E} = -\alpha[(\nabla \tfrac{1}{2}E^2) - \boldsymbol{E} \times (\nabla \times \boldsymbol{E})] \,, \quad (9.23)$$

acts onto the induced dipole. The same relation holds for an atom in an optical field. However, when averaging over a cycle of the optical oscillation the last term in (9.23) vanishes, and we obtain for the mean dipole force [9.49]

$$\langle \boldsymbol{F}_\mathrm{D} \rangle = -\frac{1}{2}\alpha \nabla (E^2) \,. \quad (9.24)$$

The polarizability $\alpha(\omega)$ depends on the frequency ω of the optical field. It is related to the refractive index $n(\omega)$ of a gas with the atomic density N (Sect. 3.1.3) by $\alpha \approx \epsilon_0(\epsilon - 1)/N$. With $(\epsilon - 1) = n^2 - 1 \approx 2(n-1)$ we obtain

$$\alpha(\omega) = \frac{2\epsilon_0[n(\omega) - 1]}{N} \,. \quad (9.25)$$

Inserting (3.37b) for $n(\omega)$, the polarizability $\alpha(\omega)$ becomes

$$\alpha(\omega) = \frac{e^2}{2m_\mathrm{e}\omega_0} \frac{\Delta\omega}{\Delta\omega^2 + (\gamma_\mathrm{s}/2)^2} \,, \quad (9.26)$$

where m_e is the electron mass, $\Delta\omega = \omega - (\omega_0 + \boldsymbol{k} \cdot \boldsymbol{v})$ is the detuning of the field frequency ω against the Doppler-shifted eigenfrequency $\omega_0 + \boldsymbol{kv}$ of the atom, and $\gamma_\mathrm{s} = \delta\omega_\mathrm{n}\sqrt{1+S}$ is the saturation-broadened linewidth characterized by the saturation parameter S (Sect. 3.6).

For $\Delta\omega \ll \gamma_\mathrm{s}$ the polarizability $\alpha(\omega)$ increases nearly linearly with the detuning $\Delta\omega$. From (9.24) and (9.26) it follows that in an intense laser beam ($S \gg 1$) with the intensity $I = \epsilon_0 c E^2$ the force $\boldsymbol{F}_\mathrm{D}$ on an induced atomic dipole is

$$\boldsymbol{F}_\mathrm{D} = -a\Delta\omega\nabla I \,, \quad \text{with} \quad a = \frac{e^2}{m\epsilon_0 c\gamma^2\omega_0 S} \,. \quad (9.27)$$

This reveals that in a homogeneous field (for example, an extended plane wave) $\nabla I = 0$ and the dipole force becomes zero. For a Gaussian beam with the beam waist w propagating in the z-direction, the intensity $I(r)$ in the x–y-plane is, according to (5.32)

$$I(r) = I_0 \, \mathrm{e}^{-2r^2/w^2} \,, \quad \text{with} \quad r^2 = x^2 + y^2 \,.$$

The intensity gradient $\nabla I = -(4r/w^2) I(r)\hat{\boldsymbol{r}}$ points into the radial direction and the dipole force $\boldsymbol{F}_\mathrm{D}$ is then directed toward the axis $r = 0$ for $\Delta\omega < 0$ and radially outwards for $\Delta\omega > 0$.

For $\Delta\omega < 0$ the z-axis of an intense Gaussian laser beam with $I(r=0) = T_0$ represents a minimum of the potential energy

$$E_{\text{pot}} = \int_0^\infty F_{\text{D}}\,\mathrm{d}r = +a\Delta\omega I_0\,, \tag{9.28}$$

where atoms with sufficiently low radial kinetic energy may be trapped. In the focus of a Gaussian beam we have an intensity gradient in the r-direction as well as in the z-direction. If the two forces are sufficiently strong, atoms can be trapped in the focal region.

Besides this dipole force in the r- and z-directions the recoil force in the $+z$-direction acts onto the atom (Fig. 9.19). In a standing wave in $\pm z$-direction the radial force and the recoil force may be sufficiently strong to trap atoms in all directions. For more details see [9.50–9.52].

Example 9.7.

In the focal plane of a Gaussian laser beam with $P_{\text{L}} = 200\,\text{mW}$ focused down to a beam waist of $w = 10\,\mu\text{m}$ ($I_0 = 1.2\times10^9\,\text{W/m}^2$), the radial intensity gradient is $\partial I/\partial r = 2r/w^2 I_0\,\mathrm{e}^{-2r^2/w^2}$, which gives for $r = w$: $(\partial I/\partial r)_{r=w} = 2I_0/w\cdot\mathrm{e}^2$. With the number above one obtains: $(\partial I/\partial r)_{r=w} = 2.4\times10^{13}\,\text{W/m}^3$ and the radial dipole force acting on a Na atom is for $\Delta\omega = -|\gamma| = -2\pi\cdot10^7\,\text{s}^{-1}$, $S = 0$, and $r = w$

$$\boldsymbol{F}_{\text{D}} = +a\Delta\omega\frac{4r}{w^2}I_0\hat{\boldsymbol{r}}_0 = 1.5\times10^{-16}\,\text{N}\,,$$

The axial intensity gradient is for a focusing lens with $f = 5\,\text{cm}$ and a beam diameter $\partial I/\partial z = 4.5\times10^5\,\text{W/m}^3$. This gives an axial dipole force of $F_{\text{D}}(z) = 3\times10^{-24}\,\text{N}$, while the recoil force is about

$$\boldsymbol{F}_{\text{recoil}} = 3.4\times10^{-20}\,\text{N}\,.$$

In the axial direction the recoil force is many orders of magnitude larger than the axial dipole force. The potential minimum with respect to the radial dipole force is $E_{\text{pot}} \simeq -5\times10^{-7}\,\text{eV}$. In order to trap atoms in this minimum their radial kinetic energy must be smaller than $5\times10^{-7}\,\text{eV}$, which corresponds to the "temperature" $T \simeq 5\times10^{-3}\,\text{K}$.

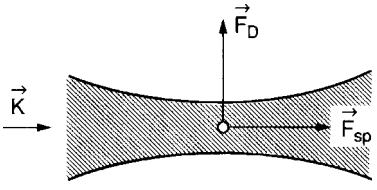

Fig. 9.19. Longitudinal and transverse forces on an atom in the focus of a Gaussian beam

Example 9.8.

Assume a standing laser wave with $\lambda = 600\,\text{nm}$, an average intensity $I = 10\,\text{W/cm}^2$, and a detuning of $\Delta\omega = \gamma = 60\,\text{MHz}$. The maximum force acting on an atom because of the intensity gradient $\nabla I = 6 \times 10^{11}\,\text{W/m}^3$ between maxima and nodes of the field becomes, according to (9.27), with a saturation parameter $S = 10$: $F_\text{D} = 10^{-17}\,\text{N}$. The trapping energy is then $1.5 \times 10^{-5}\,\text{eV} \hat{\approx} T = 0.15\,\text{K}$.

Example 9.8 demonstrates that the negative potential energy in the potential minima (the nodes of the standing wave for $\Delta\omega > 0$) is very small. The atoms must be cooled to temperatures below 1 K before they can be trapped.

Another method of trapping cooled atoms is based on the net recoil force in a three-dimensional light trap, which can be realized in the overlap region of six laser beams propagating into the six directions $\pm x$, $\pm y$, $\pm z$.

b) Magneto-Optical Trap

A very elegant experimental realization for cooling and trapping of atoms is the magneto-optical trap (MOT), which is based on a combination of optical molasses and an inhomogeneous magnetic quadrupole field (Fig. 9.21). Its principle can be understood as follows:

In a magnetic field the atomic energy levels E_i experience Zeeman shifts

$$\Delta E_i = -\boldsymbol{\mu}_i \cdot \boldsymbol{B} = -\mu_\text{B} \cdot g_F \cdot m_F \cdot B\,, \tag{9.29}$$

which depend on the Lande g-factor g_F, Bohr's magneton μ_B, the quantum number m_F of the projection of the total angular momentum F onto the field direction, and on the magnetic field B.

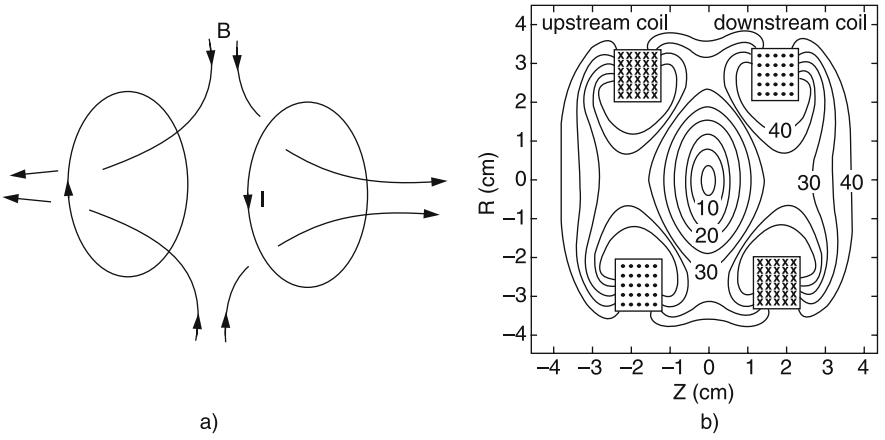

Fig. 9.20a,b. Magnetic field of the MOT: (**a**) magnetic field lines; (**b**) equipotential lines

In the MOT the inhomogeneous field is produced by two equal electric currents flowing into opposite directions through two coils with radius R and distance $D = R$ (anti-Helmholtz arrangement) (Fig. 9.20). If we choose the z-direction as the symmetry axis through the center of the coils, the magnetic field around $z = 0$ in the middle of the arrangement can be described by the linear dependence

$$B = bz \; . \tag{9.30}$$

where the constant b depends on the current through the coil and the size of the anti-Helmholtz coils. The Zeeman splittings of the transition from $F = 0$ to $F = 1$ are shown in Fig. 9.21b. Atoms in the center of this MOT are exposed to the six red-tuned laserbeams of the optical molasses (Fig. 9.21e). Let us at first only consider the two beams in the $\pm z$-direction, where the laserbeam in $+z$-direction is σ^+ polarized. Then the reflected beam in the $-z$ direction is σ^- polarized. For an atom at $z = 0$ where the magnetic field is zero, the absorption rates are equal for both laser beams, which means that the average momentum transferred to the atom is zero. For an atom at $z > 0$, however, the σ^--beam is preferentially absorbed because here the frequency

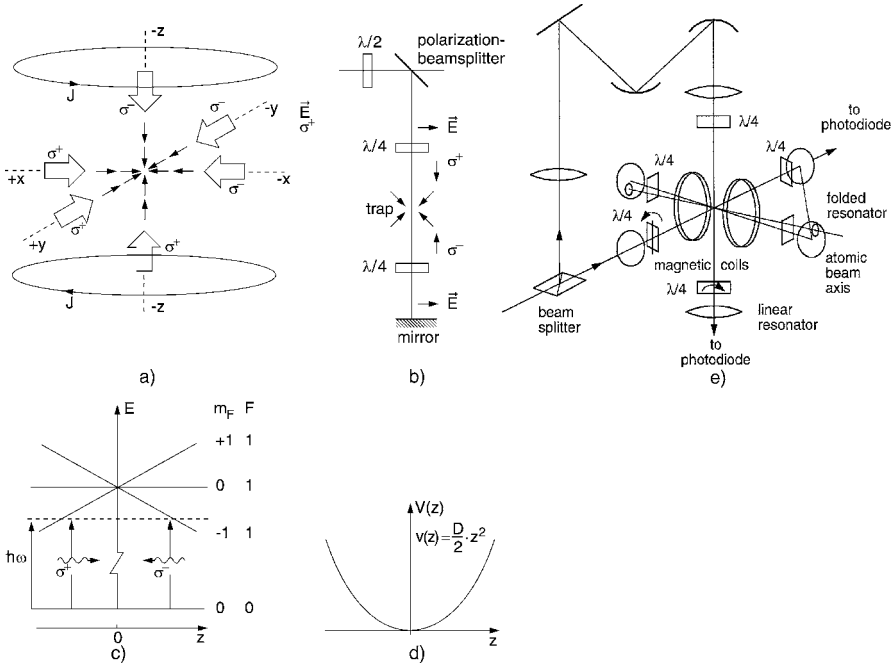

Fig. 9.21a–e. Magneto-optical trap. (**a**) Optical molasses inside the center of an inhomogeneous magnetic field; (**b**) preparation of one of the three laser beams; (**c**) level scheme illustrating the principle of the MOT; (**d**) potential of the MOT; (**e**) schematic experimental setup

difference $\omega_L - \omega_0$ is smaller than for the σ^+-beam. This means that the atom experiences a net momentum transfer into the $-z$-direction, back to the center.

In a similar way an atom at $z < 0$ shows a preferential absorption of σ^+-light and gets a net momentum in the $+z$-direction. This shows that the atoms in the MOT are compressed toward the trap center.

We will now discuss this spatially dependent restoring force more quantitatively.

From the above discussion the net force

$$\boldsymbol{F}(z) = R_{\sigma^+}(z)\hbar\boldsymbol{k}_{\sigma^+} + R_{\sigma^-}(z)\hbar\boldsymbol{k}_{\sigma^-} , \tag{9.31}$$

is determined by the difference of the absorption rates R_{σ^+}, R_{σ^-} (note that the wave vectors are antiparallel). For a Lorentzian absorption profile with halfwidth γ, the absorption rates become

$$R_{\sigma^\pm} = \frac{R_0}{1 + \left[\dfrac{\omega_L - \omega_0 \pm \mu b z/\hbar}{\gamma/2}\right]} . \tag{9.32}$$

Around $z = 0$ ($\mu b z \ll \hbar\gamma$) this expression can be expanded as a power series of $\mu b z/\hbar\gamma$.

Taking only the linear term into account yields with $\delta = \omega_L - \omega_0$:

$$F_z = -D \cdot z , \quad \text{with} \quad D = R_0 \mu \cdot b \frac{16k \cdot \delta}{\gamma^2 \left(1 + (2\delta/\gamma)^2\right)^2} . \tag{9.33}$$

We therefore obtain a restoring force that increases linearly increasing with z. The potential around the center of the MOT can be then described (because of $F_z = -\partial V/\partial z$) as the harmonic potential

$$V(z) = \frac{1}{2} D z^2 . \tag{9.34}$$

The atoms oscillate like harmonic oscillators around $z = 0$ and are spatially stabilized.

Note: There is a second force

$$F_\mu = -\boldsymbol{\mu} \cdot \operatorname{grad} \boldsymbol{B} ,$$

which acts on atoms with a magnetic moment in an inhomogeneous magnetic field.

Inserting the numbers for sodium atoms, it turns out that this force is negligibly small compared to the recoil force at laser powers in the milliwatt range. At very low temperatures, however, this force is essential to trap the atoms after the laser beams have been shut off (see Sect. 9.1.9)

In the discussion above we have neglected the velocity-dependent force in the optical molasses (Sect. 9.1.5).

The total force acting on an atom in the MOT

$$F_z = -Dz - av \,,$$

results in a damped oscillation around the center with an oscillation frequency

$$\Omega_0 = \sqrt{D/m} \,, \tag{9.35}$$

and a damping constant

$$\beta = a/m \,.$$

So far we have only considered the movement in the z-direction. The anti-Helmholtz coils produce a magnetic quadrupole field with three components. From Maxwell's equation $\operatorname{div} B = 0$ and the condition $\partial B_x/\partial x = \partial B_y/\partial y$, which follows from the rotational symmetry of the arrangement, we obtain the relations

$$\frac{\partial B_x}{\partial x} = \frac{\partial B_y}{\partial y} = -\frac{1}{2}\frac{\partial B_z}{\partial z} \,.$$

The restoring forces in the x- and y-directions are therefore half of the forces in z-directions. The trapped thermal cloud of atoms fills an ellipsoidal volume.

Instead of using counter-propagating laser beams with σ^+ and σ^- polarization, one can also cool the atoms if the two beams have the same polarization but slightly different frequencies $\omega^+ = \omega_0 + \Delta\omega$ and $\omega^- = \omega_0 - \Delta\omega$, which guarantees that the atoms moving out of the trap are pushed back. These frequencies can be produced as the two sidebands generated by acousto-optic modulation of the incident laser beam tuned to the center frequency ω_0 of the atomic transition.

Example 9.9.

With a magnetic field gradient of 0.04 T/m a sodium atom at $z = 0$ in a light trap with two counterpropagating σ^+-polarized laser beams L^+, L^- in the $\pm z$-direction with $I_+ = 0.8 I_{\text{sat}}$, $\omega_+ = \omega_0 - \gamma/2$ and $I_- = 0.15 I_{\text{sat}}$, $\omega_- = \omega_0 + \gamma/10$, the negative acceleration of a Na atom moving away from $z = 0$ reaches a value of $a = -3 \times 10^4\ \text{m/s}^2$ ($\hat{=} 3 \times 10^3 g$!), driving the atom back to $z = 0$.

Generally, the MOT is filled by slowing down atoms in an atomic beam (see Sect. 9.1.3). Spin-polarized cold atoms can also be produced by optical pumping in a normal vapor cell and trapped in a magneto-optic trap. This was demonstrated by Wieman and coworkers [9.54b], who captured and cooled 10^7 Cs atoms in a low-pressure vapor cell by six orthogonal intersecting laser beams. A weak magnetic field gradient regulates the light pressure in conjunction with the detuned laser frequency to produce a damped harmonic motion of the atoms around the potential minimum. This arrangement is far sim-

pler than an atomic beam. Effective kinetic temperatures of 1 μK have been achieved for Cs atoms. For more details on MOT and their experimental realizations see [9.6, 9.7] and [9.56].

9.1.8 Optical Cooling Limits

The lowest achievable temperatures of the trapped atoms can be estimated as follows: because of the recoil effect during the absorption and emission of photons, each atom performs a statistical movement comparable to the Brownian motion. If the laser frequency ω_L is tuned to the resonance frequency ω_0 of the atomic transition, the net damping force becomes zero. Although the time average $\langle v \rangle$ of the atomic velocity approaches zero, the mean value of $\langle v^2 \rangle$ increases, analogous to the random-walk problem [9.58, 9.59]. The optical cooling for $\omega - \omega_0 < 0$ must compensate this "statistical heating" caused by the statistical photon scattering. If the velocity of the atoms has decreased to $v < \gamma/k$, the detuning $\omega - \omega_0$ of the laser frequency must be smaller than the homogeneous linewidth of the atomic transition γ in order to stay in resonance. This yields a lower limit of $\hbar\Delta\omega < k_B T_{min}$, or with $\Delta\omega = \gamma/2$

$$T_{min} = T_D = \hbar\gamma/2k_B = \hbar/(2\tau \cdot k_B) \quad \text{(Doppler limit)}\,, \tag{9.36}$$

if the recoil energy $E_r = \hbar\omega^2(2Mc^2)^{-1}$ is smaller than the uncertainty $\hbar\gamma$ of the homogeneous linewidth.

Example 9.10.

(a) For Mg^+ ions with $\tau = 2\,\text{ns} \rightarrow \gamma/2\pi = 80\,\text{MHz}$ (9.36) yields $T_D = 2\,\text{mK}$.
(b) For Na atoms with $\gamma/2\pi = 10\,\text{MHz} \rightarrow T_D = 240\,\mu\text{K}$.
(c) For Rb atoms with $\gamma/2\pi = 5.6\,\text{MHz} \Rightarrow T_D = 140\,\mu\text{K}$.
(d) For Cs atoms with $\gamma/2\pi = 5.0\,\text{MHz} \Rightarrow T_D = 125\,\mu\text{K}$.
(e) For Ca atoms cooled on the narrow intercombination line at $\lambda = 657\,\text{nm}$ with $\gamma/2\pi = 20\,\text{kHz}$ the Doppler limit $T_D = 480\,\text{nK}$ is calculated from (9.36).

Meanwhile, experiments have shown that, in fact, temperatures lower than this calculated Doppler limit can be reached [9.60–9.62]. How is this possible?

The experimental results can be explained by the following model of *polarization gradient cooling* [9.61–9.63]. If two orthogonally polarized light waves travel anticollinearly in $\pm z$-directions through the atoms of the optical molasses in a magnetic field, the total field amplitude acting on the atoms is

$$\boldsymbol{E}(z,t) = \boldsymbol{E}_1\hat{\boldsymbol{e}}_x \cos(\omega t - kz) + E_2\hat{\boldsymbol{e}}_y \cos(\omega t + kz)\,. \tag{9.37}$$

This field shows a z-dependent elliptical polarization: for $z = 0$ it has linear polarization along the direction $\hat{\boldsymbol{e}}_1 = (\hat{\boldsymbol{e}}_x + \hat{\boldsymbol{e}}_y)$ (assuming $E_1 = E_2$), for $z = \lambda/8$ it has elliptical σ^- polarization, for $z = \lambda/4$ again linear polar-

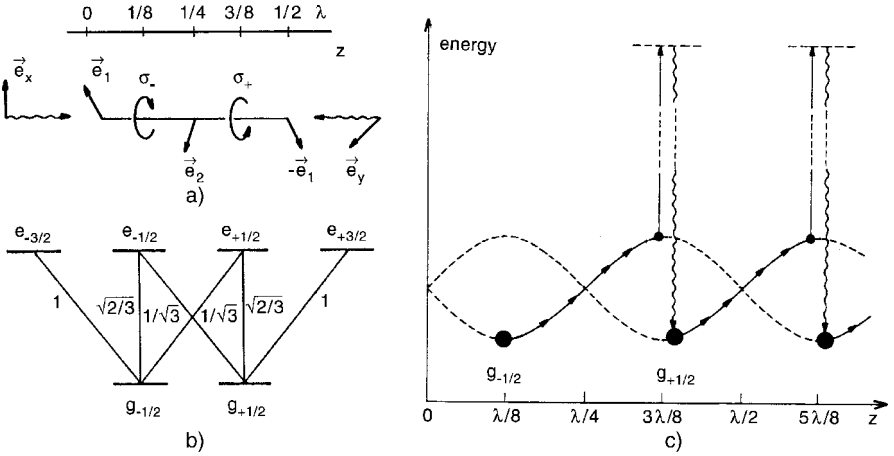

Fig. 9.22a–c. Schematic diagram of polarization gradient (Sisyphus) cooling: (**a**) two counterpropagating linearly polarized waves with orthogonal polarization create a standing wave with z-dependent polarization. (**b**) Atomic level scheme and Clebsch–Gordan coefficients for a $J_g = 1/2 \leftrightarrow J_e = 3/2$ transition. (**c**) Atomic Sisyphus effect in the lin $\perp$ lin configuration [9.61]

ization along $\hat{\boldsymbol{e}}_2 = (\hat{\boldsymbol{e}}_x - \hat{\boldsymbol{e}}_y)$, for $z = 3\lambda/8$ elliptical σ^+ polarization, etc. (Fig. 9.22a).

For an atom at rest with the level scheme of Fig. 9.22b, the energies and the populations of the two ground-state sublevels $g_{-1/2}$, $g_{+1/2}$ depend on the location z. For example, for $z = \lambda/8$ the atom rests in a σ^- light field and is therefore optically pumped into the $g_{-1/2}$ level, giving the stationary population probabilities $|(g_{-1/2})|^2 = 1$ and $|(g_{+1/2})|^2 = 0$, while for $z = (3/8)\lambda$ the atom is pumped by σ^+ light into the $g_{+1/2}$-level.

The electric field $\boldsymbol{E}(z, t)$ of the standing light wave causes a shift and broadening of the atomic Zeeman levels (*ac Stark shift*) that depends on the saturation parameter, which in turn depends on the transition probability, the polarization of $\boldsymbol{E}$, and the frequency detuning $\omega_L - \omega_0$. It differs for the different Zeeman transitions. Since the σ^- transition starting from $g_{-1/2}$ is three times as intense as that from $g_{+1/2}$ (Fig. 9.22b), the light shift Δ_- of $g_{-1/2}$ is three times the shift Δ_+ of $g_{+1/2}$. If the atom is moved to $z = (3/8)\lambda$, the situation is reversed, since now pumping occurs on a σ^+ transition.

The z-dependent energy shift of the ground-state sublevel therefore follows the curve of Fig. 9.22c. For those z values where a linearly polarized light field is present, the transition probabilities and light shifts are equal for the two sublevels.

The cooling now proceeds as follows: the important point is that the optical pumping between the sublevels takes a certain time τ_p, depending on the absorption probability and the spontaneous lifetime of the upper level. Suppose the atom starts at $z = \lambda/8$ and moves to the right with such a velocity

that it travels a distance of $\lambda/4$ during the time τ_p. Then it always climbs up the potential $E^-_{pot}(g_{-1/2})$. When the optical pumping takes place at $t = 3\lambda/8$ (which is the maximum transition probability for σ^+-light!), it is transferred to the minimum $E^+_{pot}(g_{+1/2})$ of the $g_{+1/2}$ potential and can again climb up the potential. During the optical pumping cycle it absorbs less photon energy than it emits, and the energy difference must be supplied by its kinetic energy. This means that its velocity decreases. The process is reminiscent of the Greek myth of Sisyphus, the king of Corinth, who was punished by the gods to roll a heavy rock uphill. Just before he reached the top, the rock slipped from his grasp and he had to begin again. Sisyphus was condemned to repeat this exhausting task for eternity. Therefore polarization gradient cooling is also called *Sisyphus cooling* [9.64].

Because the population density (indicated by the magnitude of the dots in Fig. 9.22c) is larger in the minimum than in the maxima of the potentials $E_{pot}(z)$, on the average the atom climbs uphill more than downhill. It transfers part of its kinetic energy to photon energy and is therefore cooled.

Depending on the polarization of the two counterpropagating laser beams the lin⊥lin configuration can be used with two orthogonal linear polarizations or the σ^+–σ^- configuration with a circularly polarized σ^+ wave, superimposed by the reflected σ^- wave. With Sisyphus cooling temperatures as low as $5-10\,\mu K$ can be achieved.

The lower limit for the achieved temperature is given by the recoil energy that each atom acquires when it emits or absorbs a photon. This recoil limit is reached when the thermal energy kT equals the recoil energy $p^2/2M = \hbar^2k^2/2M$

$$k_B T_{recoil} = \hbar^2 k^2/2M = h^2/(\lambda^2 \cdot 2M), \tag{9.38}$$

where M is the mass of the atom and $\hbar\boldsymbol{k}$ the momentum of the photon.

Example 9.11.
For Na atoms $m = 23$ AMU, $\lambda = 589\,nm \rightarrow T_{recoil} = 1.1\,\mu K$. This is 220 times lower than the Doppler limit.

The recoil limit can be overcome by a recently discovered cooling scheme called Raman cooling (Fig. 9.23). Here a stimulated Raman scattering process is used, which traverses from level 1 via a virtual level down to level 3. If the levels 1 and 3 are hyperfine components of the electronic groundstate, the energy difference between 1 and 3 is very small compared to $h\nu$. Since the energies of the exciting photon and Raman photon are nearly equal, the absorption and emission recoils cancel each other out because both photons travel in the same direction. Since the Stokes photon has a slightly smaller momentum than the incident photon, this small difference results in a cooling of the translational energy of the atom. Because no fluorescence photon is emitted, the statistically varying recoil present for Sysiphos cooling is missing here, so the cooling limit can be pushed further down.

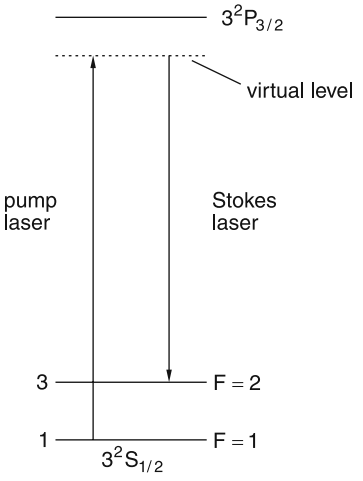

Fig. 9.23. Level scheme for Raman cooling

Review articles about laser cooling can be found in [9.65–9.67].

9.1.9 Bose–Einstein Condensation

At sufficiently low temperatures where the de Broglie wavelength

$$\lambda_{\mathrm{DB}} = \frac{h}{m \cdot v} , \tag{9.39}$$

becomes larger than the mean distance $d = n^{-1/3}$ between the atoms in the cold gas with density n, a phase transition takes place for bosonic particles with integer total spin. More and more particles occupy the lowest possible energy state in the trap potential and are then indistinguishable, which means that all these atoms in the same energy state are described by the same wave function (note that for bosons the Pauli exclusion principle does not apply). Such a situation of a macroscopic state occupied by many indistinguishable particles is called a *Bose–Einstein condensate* (BEC, Nobel prize in physics 2001 for E. Cornell, W. Ketterle, and C. Wiemann).

More detailed calculations show that BEC is reached if

$$n \cdot \lambda_{\mathrm{DB}}^3 > 2.612 . \tag{9.40}$$

With $v^2 = 3k_{\mathrm{B}}T/m$ we obtain the de Broglie wavelength

$$\lambda_{\mathrm{DB}} = \frac{h}{\sqrt{3mK_{\mathrm{B}}T}} , \tag{9.41}$$

and the condition (9.41) for the critical density becomes

$$n > 13.57(m \cdot k_{\mathrm{B}}T)^{3/2}/h^3 .$$

The minimum density for BEC depends on the atomic mass and on the temperature and decreases with $T^{3/2}$ [9.6, 9.68].

Example 9.12.

For Na atoms at a temperature of $10\,\mu K$ the critical density would be $n = 6 \times 10^{14}\,/cm^3$, which is at present not achievable. For experimentally realized densities of $10^{12}\,cm^{-3}$ the atoms have to be cooled below 100 nK in order to reach BEC.

For rubidium atoms BEC was observed at $T = 170\,nK$ and a density of $3 \times 10^{12}\,cm^{-3}$.

9.1.10 Evaporative Cooling

The temperatures reached with the optical cooling methods discussed so far are not sufficiently low to obtain Bose–Einstein condensation. Here the very old and well-known technique of evaporation cooling leads to the desired goal. The principle of this method is as follows [9.69]:

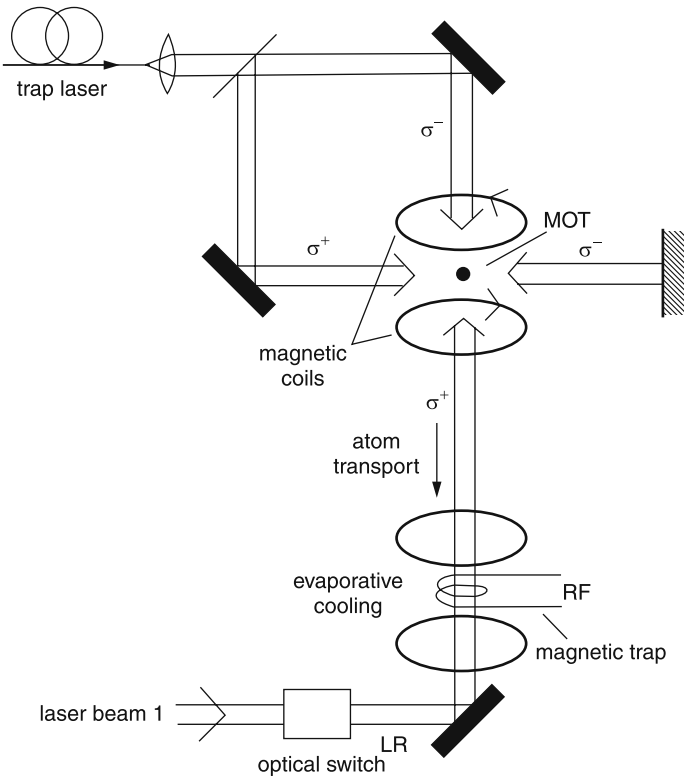

Fig. 9.24. Schematic experimental setup for optical cooling in the MOT; atom transport is achieved in the magnetic trap by switching off laser beam 1

The optically cooled atoms are transferred from the MOT to a purely magnetic trap (Fig. 9.24), where the restoring force

$$\boldsymbol{F} = \mu \mathrm{grad}\, \boldsymbol{B}\,,$$

keeps the cold atoms in a cloud around the minimum of the potential energy $W = -\mu \cdot B$ at the center of the magnetic trap. The total energy of the atoms is $W = W_{\mathrm{pot}} + W_{\mathrm{kin}}$. The atoms with the highest kinetic energy occupy the highest energy levels of the trap. Now the particles with the highest energy are removed from the trap, thus perturbing the equilibrium velocity distribution. This is achieved by a radio-frequency field that induces spin flips and thus reverses the sign of the force, changing it from a restoring to a repellent force. This is shown in Fig. 9.25b in a potential diagram. If the remaining atoms suffer sufficient mutual collisions, a new equilibrium state is reached

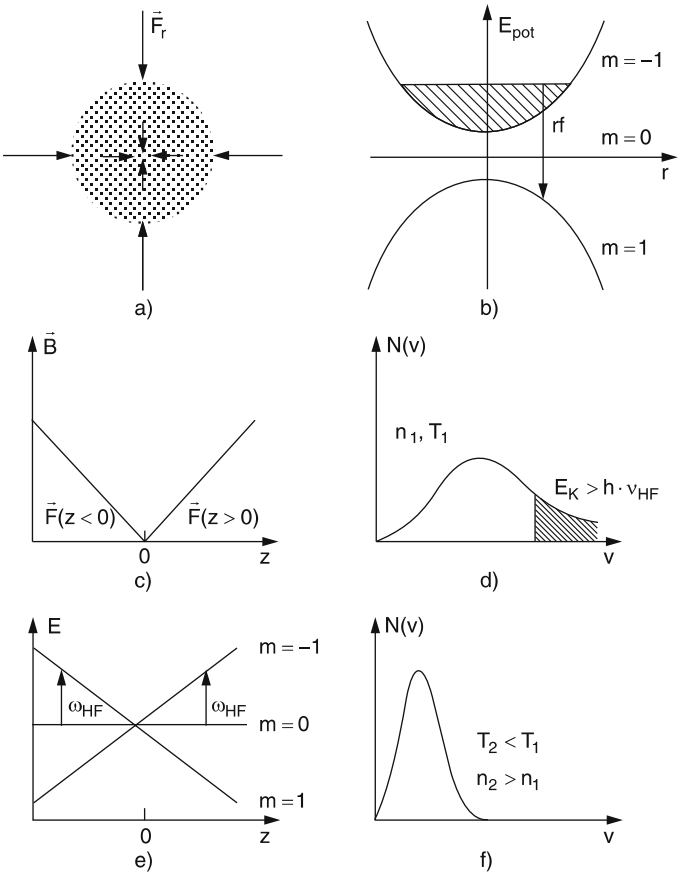

Fig. 9.25a–f. Evaporative cooling of a cold atom cloud in a magnetic field. (**a**) Optical molasses; (**b**) trap potential; (**c**) magnetic field $B(z)$; (**d**) Boltzmann distribution before evaporative cooling; (**e**) HF transitions; (**f**) $N(v)$ after evaporation cooling

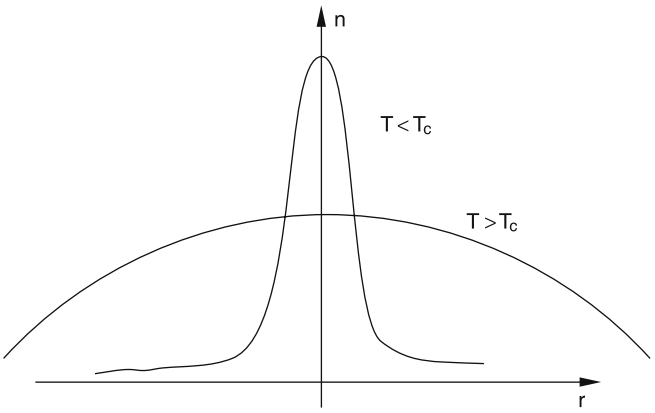

Fig. 9.26. Radial density profile for cooled atoms in a magnetic trap above and below the critical phase transition temperature T_c

with a lower temperature. Again, the upper part of the Maxwellian velocity distribution is thrown out of the trap. Lowering the radio frequency continuously always results in a loss of the atoms with the highest kinetic energy, which reach the largest distance from the trap center and therefore have the largest Zeeman splittings.

The cooling process must be slow enough to maintain thermal equilibrium, but should be sufficiently fast in order not to lose particles from the trap by collision-induced spin flips.

The phase transition to BEC manifests itself by the sudden increase of the atomic density (Fig. 9.26), which can be monitored by measuring the absorption of an expanded probe laser beam (Fig. 9.27).

The BEC can be kept only for a limited time. There are several loss mechanisms that result in a decay of the trapped particle density. These are spin-flip

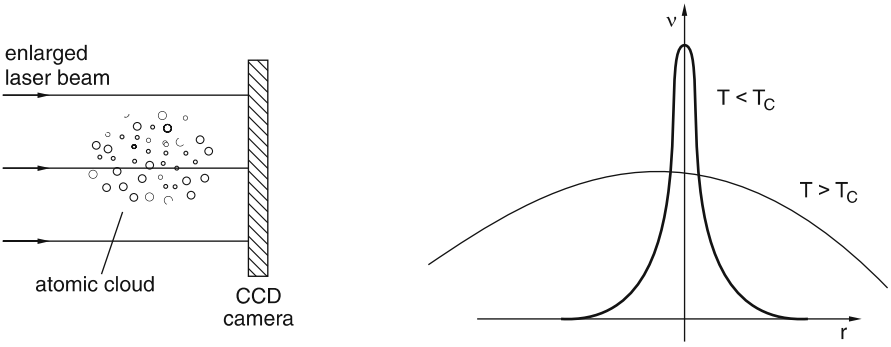

Fig. 9.27. (**a**) Measurement of spatial extension and radial density profile of the cold atomic cloud through the absorption of an enlarged weak laser beam. (**b**) Radial density profiles above and below the critical phase transition temperature T_c

collisions, three-body recombination where molecules are formed, collisions with excited atoms where the excitation energy may be converted into kinetic energy, and collisions with rest gas atoms or molecules. The background pressure therefore has to be as low as possible (typical pressures are 10^{-10} to 10^{-11} mbar)

The scattering length a of the atoms in the BEC determines the elastic cross section $\sigma_{el} = 8\pi a^2$. The value of a is positive for a repulsive mean potential of the condensate. For negative scattering lengths the condensate will finally collapse.

It is interesting to note that the value of the scattering length a for atoms A can be obtained from laser spectroscopy by measuring the energy and the vibrational wave function of the last bound vibrational level in the ground-state potential of the molecule A_2 [9.70].

9.1.11 BEC of Molecules

Recently the Bose–Einstein condensation of diatomic molecules has even been reported [9.71]. At first sight this appears astonishing, because molecules do not represent two-level systems and therefore cannot be optically cooled like atoms. One must therefore look for other cooling schemes. We will discuss some of them here.

A promising way to produce cold molecules is the photoassociation of cold atoms in a Bose–Einstein condensate, which was discussed in Sect. 5.5.6. Here cold molecules in stable higher vibrational levels of the electronic ground state can be produced with very low translational energy.

Another method is based on the sympathetic cooling of molecules in a cold atomic gas which does not react with the molecules but cools their translational energy down to the atomic temperature.

A very elegant method that was finally successfully used to generate molecular BECs uses the difference in the potential energy of atoms with electron spin and molecules in a magnetic field [9.71]. In Fig. 9.28, the energy of a collision pair Cs + Cs with parallel electron spins and that of the molecule Cs_2 is plotted as a function of the magnetic field strength B. The field dependence $E(B)$ is stronger for the collision pair with the atoms in hyperfine levels with the quantum numbers $F = 3$; $M_F = 3$; $L = 0$ and the magnetic moment $\mu = 1.5\mu_B$ than for the molecule in the $4g$ hyperfine level with $F = 4$ and $\mu = 0.93\mu_B$. At a critical field strength B_c the two lines cross each other. This means that a molecular level exists which has the same energy as the collision pair (Feshbach resonance; see the inset in Fig. 9.28). On the left side of the Feshbach resonance, the molecular state has a lower energy and thus stable molecules can be formed. If the magnetic field is slowly (adiabatically) scanned from higher field strengths across the Feshbach resonance to lower values, stable molecules can be produced. This is monitored by the corresponding decrease in the atomic density in the BEC. When the field strength is again increased to higher values above B_c, the atomic density increases again, which means that the molecules dissociate.

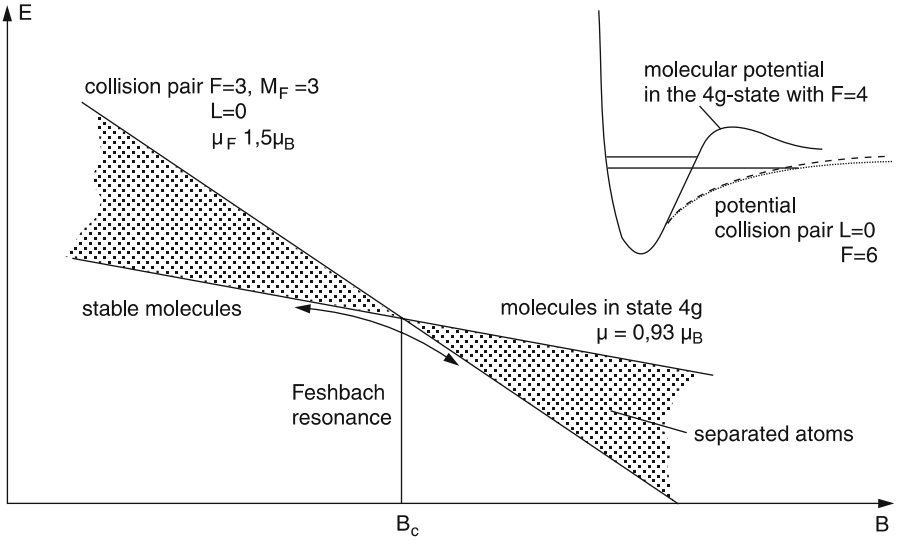

Fig. 9.28. Potential energy of the collision pair $Cs(F = 3, M_F = 3) + Cs(F = 3, M_F = 3)$ and the molecule Cs_2 as a function of an external magnetic field [9.73]

Since the dimer Cs_2 has an integer total spin, it is a boson and can form a Bose–Einstein condensate [9.72]. Spectroscopy of these dimers, which represent huge molecules with an internuclear separation of about 100 nm (!) gives information on the energy of the last bound molecular levels directly below the dissociation energy. Often such levels are only stabilized by the centrifugal barrier for states with rotational quantum numbers $J > 0$. The binding energies of these states allow more detailed analysis of the different contributions to the long-range forces of weakly bound systems [9.73].

Feshbach-like resonances in a molecular cesium BEC indicate that even molecular dimers $(Cs_2)_2$ can be formed from the atomic dimers Cs_2 when the magnetic field is tuned over molecular resonances [9.74a].

9.1.12 Applications of Cooled Atoms and Molecules

Optical cooling and deflection of atoms open new areas of atomic and molecular physics. Collisions at very small relative velocities, where the deBroglie wavelength $\lambda_{DB} = h/(mv)$ is large, can now be studied. They give information about the long-range part of the interaction potential, where new phenomena arise, such as retardation effects and magnetic interactions from electron or nuclear spins [9.74b,c]. One example is the study of collisions between Na atoms in their $3\,^2S_{1/2}$ ground state. The interaction energy depends on the relative orientation of the two electron spins $S = \frac{1}{2}$. The atoms with parallel spins form a Na_2 molecule in a $^3\Sigma_u$ state, while atoms with antiparallel spins form a $Na_2(^1\Sigma_g^+)$ molecule. At large internuclear distances ($r > 1.5$ nm) the energy

differences between the $^3\Sigma_u$ and $^1\Sigma_g$ potentials become comparable to the hyperfine splitting of the Na($3\,^2S_{1/2}$) atoms [9.75]. The interaction between the nuclear spins and the electron spins leads to a mixing of the $^3\Sigma_u$ and $^1\Sigma_u$ states, which corresponds in the atomic model of colliding atoms to *spin-flip* collisions (Fig. 9.29).

Collisions between cold atoms in a trap can be studied experimentally by measuring the loss rate of trapped atoms under various trap conditions (temperature, magnetic-field gradients, light intensity, etc.). It turns out that the density of excited atoms cannot be neglected compared with the density of ground-state atoms, and the interaction between excited- and ground-state atoms plays an essential role. For collisions at very low temperatures the absorption and emission of photons during the collisions is important, because the collision time $\tau_c = R_c/v$ becomes very long at low relative atomic velocities v. The two dominant energy-transfer processes are collision-induced fine-structure transitions in the excited state and radiative redistribution, where a photon is absorbed by an atom at the position $\boldsymbol{r}_1$ in the trap potential $V(\boldsymbol{r})$ and another photon with a slightly different energy is reemitted after the atom has moved to another position $\boldsymbol{r}_2$.

Another application is the deflection of atoms by photon recoil. For sufficiently good beam collimation, the deflection from single photons can be detected. The distribution of the transverse-velocity components contains information about the statistics of photon absorption [9.76]. Such experiments have successfully demonstrated the antibunching characteristics of photon ab-

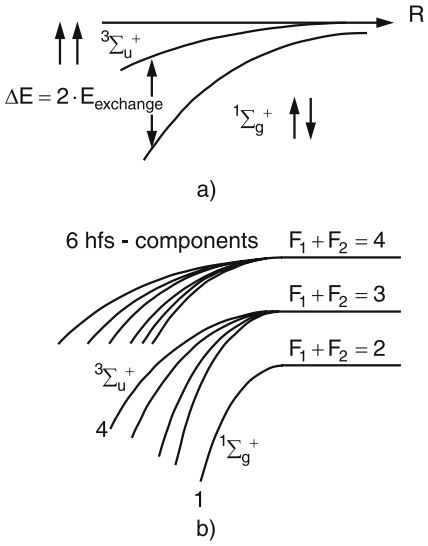

Fig. 9.29a,b. Interaction between two Na atoms at large internuclear distances R for different spin orientations: (**a**) without hyperfine structure and (**b**) including the nuclear spins $I = (3/2)\hbar$, which gives three dissociation limits

sorption [9.77]. The photon statistic is directly manifest in the momentum distribution of the deflected atoms [9.78]. Optical collimation by radial recoil can considerably decrease the divergence of atomic beams and thus the beam intensity. This allows experiments in crossed beams that could not be performed before because of a lack of intensity.

A very interesting application of cold trapped atoms is their use for an optical frequency standard [9.79]. They offer two major advantages: reduction of the Doppler effect and prolonged interaction times on the order of 1 s or more. Optical frequency standards may be realized either by atoms in optical traps or by atomic fountains [9.80].

For the realization of an atomic fountain, cold atoms are released in the vertical direction out of an atomic trap. They are decelerated by the gravitational field and return back after having passed the culmination point with $v_z = 0$.

Example 9.13.

Assume the atoms start with $v_{0z} = 5\,\mathrm{m/s}$. Their upward flight time is then $t = v_{0z}/g = 0.5\,\mathrm{s}$, their path length is $z = v_0 t - gt^2/2 = 1.25\,\mathrm{m}$, and their total flight time is 1 s. Their transit time through a laser beam with the diameter $d = 1\,\mathrm{cm}$ close to the culmination point is $T_{\mathrm{tr}} = 90\,\mathrm{ms}$, and the maximum transverse velocity is $v \leq 0.45\,\mathrm{m/s}$. The transit-time broadening is then less than 10 Hz.

There are many possible applications of cold trapped molecules.

One example is the spectroscopy of highly forbidden transitions, which becomes possible because of the long interaction time. Another aspect is a closer look at the chemistry of cold trapped molecules, where the reaction rates and the molecular dynamics are dominated by tunneling and a manipulation of molecular trajectories seems possible. Experiments on testing time-reversal symmetry via a search for a possible electric dipole moment of the proton or the electron [9.81] are more sensitive when cold molecules are used [9.82, 9.83].

9.2 Spectroscopy of Single Ions

During recent years it has become possible to perform detailed spectroscopic investigations of single ions that are stored in electromagnetic (EM) traps and cooled by special laser arrangements. This allows tests of fundamental problems of quantum mechanics and electrodynamics and, furthermore, opens possibilities for precise frequency standards.

9.2.1 Trapping of Ions

Since ions show stronger interactions with EM fields than neutral atoms, which experience only a weak force because of their polarizability, they